NASA CR-134917

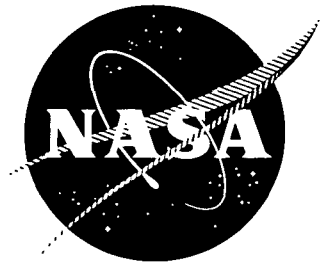

AMPLIFICATION OF REYNOLDS NUMBER DEPENDENT PROCESSES BY WAVE DISTORTION - JUNE 1975 PROGRESS REPORT

by

Marie B. Ventrice, Jih-Chin Fang
and
Kenneth R. Purdy

Department of Mechanical Engineering
Tennessee Technological University
Cookeville, Tennessee 38501

prepared for

NATIONAL AERONAUTICS AND SPACE ADMINISTRATION

NASA Lewis Research Center
Grant NGR 43-003-015
Richard J. Priem, Technical Officer

NOTICE

This report was prepared as an account of Government-sponsored work. Neither the United States, not the National Aeronautics and Space Administration (NASA), nor any person acting on behalf of NASA:

A) Makes any warranty or representation, expressed or implied, with respect to the accuracy, completeness, or usefulness of the information contained in this report, or that the use of any information, apparatus, method, or process disclosed in this report may not infringe privately-owned rights; or

B) Assumes any liabilities with respect to the use of, or for damages resulting from the use of, any information, apparatus, method or process disclosed in this report.

As used above, "person acting on behalf on NASA" includes any employee or contractor of NASA, or employee of such contractor, to the extent that such employee or contractor of NASA or employee of such contractor prepares, disseminates, or provides access to any information pursuant to his employment or contract with NASA, or his employment with such contractor.

1. Report No.	2. Government Accession No.	3. Recipient's Catalog No.
CR-134917		

4. Title and Subtitle	5. Report Date
AMPLIFICATION OF REYNOLDS NUMBER DEPENDENT PROCESSES BY WAVE DISTORTION - JUNE 1975 PROGRESS REPORT	June 1975
	6. Performing Organization Code

7. Author(s)	8. Performing Organization Report No.
Marie B. Ventrice, Jih-Chin Fang and Kenneth R. Purdy	
	10. Work Unit No.

9. Performing Organization Name and Address	11. Contract or Grant No.
Department of Mechanical Engineering Tennessee Technological University Cookeville, Tennessee 38501	NGR 43-003-015
	13. Type of Report and Period Covered Progress Report July 1974 - June 1975

12. Sponsoring Agency Name and Address	14. Sponsoring Agency Code
National Aeronautics and Space Administration Washington, DC 20546	

15. Supplementary Notes

Technical Officer, Richard J. Priem, Combustion Technology Section
NASA Lewis Research Center, Cleveland, Ohio 44135

16. Abstract

A system using a hot-wire transducer as an analog of a liquid droplet of propellant was employed to investigate the ingredients of the acoustic instability of liquid-propellant rocket engines. It was assumed that the combustion process was vaporization-limited and that the combustion chamber was acoustically similar to a closed-closed right-circular cylinder.

Before studying the hot-wire closed-loop system (the analog system), a microphone closed-loop system, which used the response of a microphone as the source of a linear feedback exciting signal, was investigated to establish the characteristics of self-sustenance of acoustic fields. Self-sustained acoustic fields were found to occur only at resonant frequencies of the chamber. The factors that determined the character of the self-sustenance were found to be the phase between the existing and feedback acoustic fields and the feedback-loop gain. The form of the initial exciting acoustic field did not influence either the form or the level of the resultant self-sustained acoustic field.

In the hot-wire closed-loop system, the response of hot-wire anemometer was used as the source of the feedback exciting signal. The self-sustained acoustic fields which developed in the system were always found to be harmonically distorted and to have as their fundamental frequency a resonant frequency for which there also existed a second resonant frequency which was approximately twice the fundamental frequency. The factors that determined self-sustenance were found to be the phase between the existing and feedback acoustic fields at each of the harmonic components and the feedback-loop gain. The form of the initial exciting acoustic field did not influence the form of the resultant self-sustained acoustic field; however, it did influence the gain required and, consequently, the level of the resultant self-sustained acoustic field.

For a hot-wire transducer, both theoretical analysis and experimental observation showed that the response of the heat-transfer process to an acoustic field was nonlinear. When the acoustic field consisted of a single resonant frequency, the response was dominated by a frequency twice that of the acoustic field. However, when the acoustic field was harmonically distorted, the response contained a fundamental frequency component as well as higher harmonic components. This nonlinear character was found to be the cause of the wave distortion and the basic means for self-sustenance of the acoustic field. The results of this study were interpreted in terms of combustion instability.

17. Key Words (Suggested by Author(s))	18. Distribution Statement
Combustion instability Resonance Acoustics Nonlinear response	Unclassified - Unlimited

19. Security Classif. (of this report)	20. Security Classif. (of this page)	21. No. of Pages	22. Price*
Unclassified	Unclassified	55	$3.00

* For sale by the National Technical Information Service, Springfield, Virginia 22151

FOREWORD

This is a status report covering research conducted during the twelve-month period ending 30 June 1975. The investigations described herein were sponsored by the National Aeronautics and Space Administration, Lewis Research Center, Cleveland, Ohio 44135, under grant number NGR 43-003-015. It was administered under the technical cognizance of Dr. Richard J. Priem, Head of the Combustion Technology Section. Dr. Priem's interest in the work is deeply appreciated.

The report is based upon the doctoral research of Jih-Chin Fang and was conducted under the supervision of Dr. Purdy, the principal investigator.

Support was also given to the project by the Department of Mechanical Engineering. This crucial help is gratefully acknowledged.

AMPLIFICATION OF REYNOLDS NUMBER DEPENDENT PROCESSES BY WAVE DISTORTION

INTRODUCTION

It is difficult to study the high frequency combustion instability which sometimes occurs during the operation of developmental liquid-propellant rocket engines. Because of this, it was proposed that an analog device—the output of a constant-temperature hot-wire anemometer (CTHWA)—be used for such a study. Both the energy release of the vaporization-limited combustion process in a liquid-propellant rocket engine and the CTHWA output are modeled as being Reynolds number dependent.

The energy release rate (burning rate) in vaporization-limited combustion is equal to the vaporization rate of the liquid-propellant droplets. The equation for vaporization rate, as given by Priem and Heidmann [1], is

$$W = C_1 + C_2 \, Re^{0.5} \tag{1}$$

where

$$C_1 = \frac{2\pi D M_\ell \mathcal{D} C_d}{R_u T} P \ln \frac{P}{P-P_v} \tag{2}$$

$$C_2 = \frac{0.6 \, Sc^{0.33} \pi D M_\ell \mathcal{D} C_d}{R_u T} P \ln \frac{P}{P-P_v} \tag{3}$$

and

$$Re = \frac{\rho D|\vec{V} - \vec{V}_d|}{\mu} \tag{4}$$

The Reynolds number is based upon the propellant droplet diameter and relative velocity between the droplet and the surrounding gases. Coefficients C_1 and C_2 depend upon the properties of the gases and the droplet.

The heat transfer rate from a hot wire, based upon a correlation equation developed by Collis and Williams [2], has been shown by Fang [3] to be

$$\dot{Q} = C_3 + C_4 \, Re_f^m \tag{5}$$

where

$$C_3 = \pi L_w k_f [T_f/T]^{0.17} \, [T_w - T]A \tag{6}$$

$$C_4 = \pi L_w k_f [T_f/T]^{0.17} \, [T_w - T]B \tag{7}$$

and the Reynolds number, evaluated at the film temperature, is

$$Re_f = \frac{\rho_f D_w |\vec{V}|}{\mu_f} \tag{8}$$

The Reynolds number is based upon the hot-wire diameter and the velocity of the surrounding gas relative to the hot wire. Coefficients C_3 and C_4 depend upon the properties of the gas and the hot wire.

In addition, it has been shown by Fang [3] that the heat transfer rate $\dot{Q}$ is proportional to the square of the voltage output E from the

anemometer, or

$$E^2 = C_5\dot{Q} = C\,[C_3 + C_4\,Re_f^{\,m}] \tag{9}$$

where

$$C_5 = [R_w + R_{cbl} + R_p + R_s]^2/R_w \tag{10}$$

In a simplified form, Figure 1 compares the closed-loop analog process to the closed-loop combustion process. In a liquid-propellant rocket engine, an unsteady flow field surrounding a fuel droplet produces unsteady vaporization and burning of the fuel droplet, which produces an unsteady flow field. This combines with the previous unsteady flow field and, thereby, closes the loop. For the CTHWA, an unsteady flow field surrounding the hot wire produces unsteady heat transfer from the wire, which produces an unsteady output voltage from the anemometer, which produces an unsteady acoustic driver output. This produces an unsteady flow field around the hot wire, which then combines with the previous unsteady flow field and, thereby, closes the loop. One of the most important aspects of the closed-loop behavior is how the initial and feedback oscillations combine to form new gas oscillations. The importance of comparing the initial and feedback oscillations in a system was suggested by Rayleigh [4]. In his work, originally published in 1878, he postulated that if an oscillatory heat source had a component of its rate in phase with an acoustic oscillation, the acoustic oscillation would be amplified. This is known as Rayleigh's criterion.

An estimate of the normal closed-loop behavior of the two systems has been made by means of an open-loop analysis. The open-loop analysis

CLOSED-LOOP FEEDBACK SYSTEMS

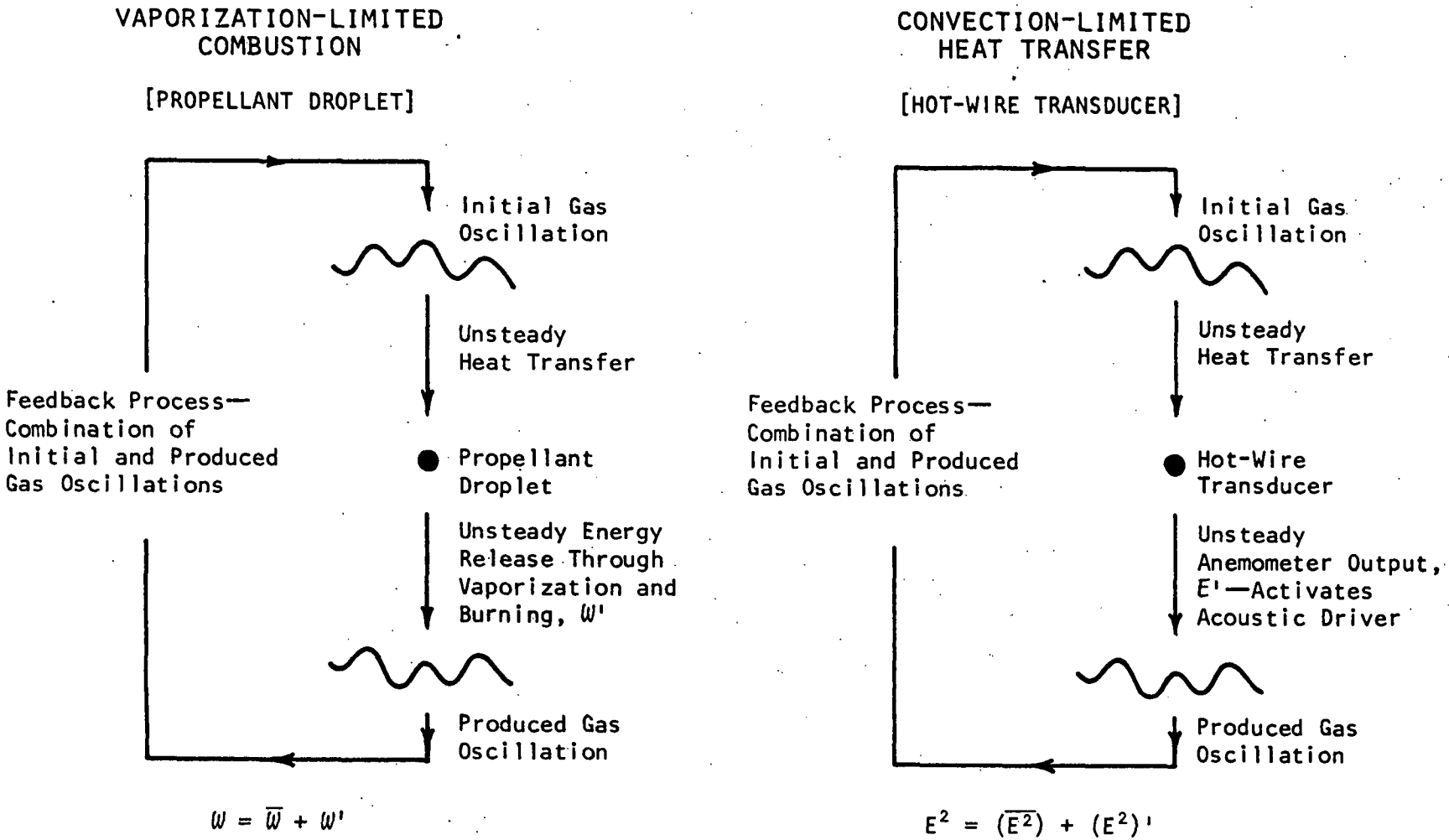

Figure 1. Combustion and Anemometer Closed-Loop Models

consists of comparing the output of the process (burning rate in the case of vaporization limited combustion, voltage in the case of the CTHWA) to the input (acoustic pressure). The quantity obtained from this comparison is the open-loop response factor; it is an indication of whether the acoustic gains of the system are sufficient to overcome the acoustic losses and cause instability.

Heidmann [5] analytically performed a response factor analysis of the combustion process. Purdy, Ventrice and Fang [6] analytically performed a response factor analysis of the analog process; and, in addition, Ventrice and Purdy [7] carried out an experimental investigation of the response of the analog process.

The same general results were obtained in all three investigations. If the system is perturbed by a sinusoidal disturbance, the response is low and the system is predicted to be stable; adding distortion to the sinusoidal disturbance, in the form of a sinusoid at double the original frequency, can cause higher response factors, high enough that instability is predicted. The amplitude and phase of the distortion sinusoid, relative to the original (fundamental) sinusoid, dominate the factors which control the increase in the response.

The results obtained in all three studies were in agreement with observations made during actual unstable rocket combustion. The vibrations which occur during unstable combustion can be characterized as a sinusoid at a fundamental frequency distorted by a sinusoid at twice the fundamental frequency. Other higher harmonic components exist, but are small compared to the fundamental and second harmonic components. All the studies indicate that a distortion component is necessary in order to have unstable combustion; however, the studies do

not clearly indicate why the distortion component is needed.

In an effort to obtain further insight into the causes and control of combustion instability, and why a distortion component is necessary, the open-loop studies with the analog process have been extended to include an investigation of the actual closed-loop interaction between the heat-transfer process and the gas-dynamic variables of the system. Earlier experimental work [7] had indicated that the acoustic characteristics of the test chamber itself had a strong influence on the type of instability which would develop; therefore, this aspect was studied in detail.

To carry out the research, a closed-closed cylindrical test chamber was used. Acoustic drivers were mounted on the chamber to generate the necessary acoustic vibrations in the chamber. The sensor (hot-wire transducer) of the CTHWA was mounted in the chamber; and, in addition, microphones were located at various places in the chamber walls to monitor the acoustic pressure. A number of pieces of electronic equipment were used to time delay or phase shift the output signal from the CTHWA, amplify it and feed it back to the acoustic drivers to permit velocity-dependent closed-loop operation of the system. A microphone was also used as the sensor to form a pressure-dependent closed-loop system for comparison purposes.

Various types of closed-loop operation were examined to determine how the system would react—would a disturbance die out, increase in intensity, transition to some other form, remain stable for long periods of time or follow some other pattern of behavior? When the vibrations in a system could sustain themselves during closed-loop operation, the significant parameters were investigated to determine

the mechanisms enabling this self-sustenance. Concomitant to these investigations, analytical and experimental fourier series analyses were made of the output of the CTHWA when the hot wire was exposed to various sound fields.

The investigations and results reported here are a condensation of a dissertation by Fang [3].

THEORETICAL INVESTIGATIONS

Gas in a chamber will react most strongly to vibrations at the chamber's resonant frequencies; therefore, a knowledge of the characteristics of the solution of the inviscid wave equation for the gas in the cylindrical enclosure used in these studies was necessary for an understanding of both theoretical and experimental analyses. The assumptions, boundary conditions, equations and details of the solution are given by Fang [3]. The solution yields the frequencies of the natural modes of acoustic vibration of a gas in a closed-closed cylindrical chamber and the equations for the acoustic pressure, temperature, density and velocity when the gas is excited at these frequencies.

The resonant frequencies of vibration of a gas in a closed-closed cylindrical chamber are determined by the eigen values of the solution and are

$$f_{mnn_z} = \frac{\omega_{mnn_z}}{2\pi} = \frac{C_\infty}{2}\left[\left(\frac{\alpha_{mn}}{R}\right)^2 + \left(\frac{n_z}{L}\right)^2\right]^{0.5} \qquad (11)$$

where m, n and n_z are tangential, radial and longitudinal mode numbers,

respectively. (Hereafter, gas vibration at the frequency f_{mnn_z} will be referred to as $<mnn_z>$ vibration, or just $<mnn_z>$.)

The equations for the pressure, temperature, density and velocity components during $<mnn_z>$ vibration are:

$$P'_{mnn_z} = \hat{P}_{mnn_z} \frac{J_m(\alpha_{mn}\pi r/R)}{J_m(\alpha_{mn}\pi)} \cos(n_z\pi z/L)\cos(m\theta)\sin(\omega_{mnn_z} t - \phi_{mnn_z}) \qquad (12)$$

$$T'_{mnn_z} = \frac{\hat{P}_{mnn_z} T_\infty(\gamma-1)}{C_\infty^2 \rho_\infty} \frac{J_m(\alpha_{mn}\pi r/R)}{J_m(\alpha_{mn}\pi)} \cos(n_z\pi z/L)\cos(m\theta)\sin(\omega_{mnn_z} t - \phi_{mnn_z}) \qquad (13)$$

$$\rho'_{mnn_z} = \frac{\hat{P}_{mnn_z}}{C_\infty^2} \frac{J_m(\alpha_{mn}\pi r/R)}{J_m(\alpha_{mn}\pi)} \cos(n_z\pi z/L)\cos(m\theta)\sin(\omega_{mnn_z} t - \phi_{mnn_z}) \qquad (14)$$

$$V'_{r_{mnn_z}} = \frac{\hat{P}_{mnn_z} \alpha_{mn}\pi}{\rho_\infty \omega_{mnn_z} R} \frac{J'_m(\alpha_{mn}\pi r/R)}{J_m(\alpha_{mn}\pi)} \cos(n_z\pi z/L)\cos(m\theta)\cos(\omega_{mnn_z} t - \phi_{mnn_z}) \qquad (15)$$

$$V'_{\theta_{mnn_z}} = -\frac{\hat{P}_{mnn_z} m}{\rho_\infty \omega_{mnn_z} r} \frac{J_m(\alpha_{mn}\pi r/R)}{J_m(\alpha_{mn}\pi)} \cos(n_z\pi z/L)\sin(m\theta)\cos(\omega_{mnn_z} t - \phi_{mnn_z}) \qquad (16)$$

$$V'_{z_{mnn_z}} = -\frac{\hat{P}_{mnn_z} n_z\pi}{\rho_\infty \omega_{mnn_z} L} \frac{J_m(\alpha_{mn}\pi r/R)}{J_m(\alpha_{mn}\pi)} \sin(n_z\pi z/L)\cos(m\theta)\cos(\omega_{mnn_z} t - \phi_{mnn_z}) \qquad (17)$$

In a rocket combustion chamber during unstable operation, tangential modes of acoustic vibration appear to be dominant. A tangential type vibration can occur in two forms—standing or spinning. Figure 2 illustrates the differences in the characteristic acoustic pressure and velocity distributions for <100> standing and spinning vibrations. The top line illustrates the pressure distribution along the horizontal diameter at various times during a cycle; it is the same for standing and spinning forms. The remainder of the illustration shows the acoustic pressure and velocity distributions over the entire cross-section at various times; note that these are not the same for standing and spinning forms. On the pressure illustrations, the dashed lines indicate the pressure is below ambient and the solid lines indicate the pressure is above ambient. The spinning form of tangential vibration normally occurs during unstable combustion; however, mathematically, the spinning vibration is the sum of two standing vibrations which are out of phase by a quarter of a period in time and which have their pressure antinodal points located 90 degrees apart in space.

As discussed earlier, the acoustic vibrations which occur during unstable combustion can be characterized by a sinusoid at a fundamental frequency, distorted by a sinusoid at twice the fundamental frequency. To simulate these characteristics, the chamber used was designed so that $f_{202} = 2f_{100}$. If a <100> and a <202> vibration occur simultaneously in a chamber, the acoustic pressure variations at a particular location in the chamber will be the sum of two sinusoids—selecting a particular location fixes the values of r, θ and z, and selecting the modes of vibration determines the values of m, n and n_z, the only variable remaining in the equation for the acoustic pressure is time.

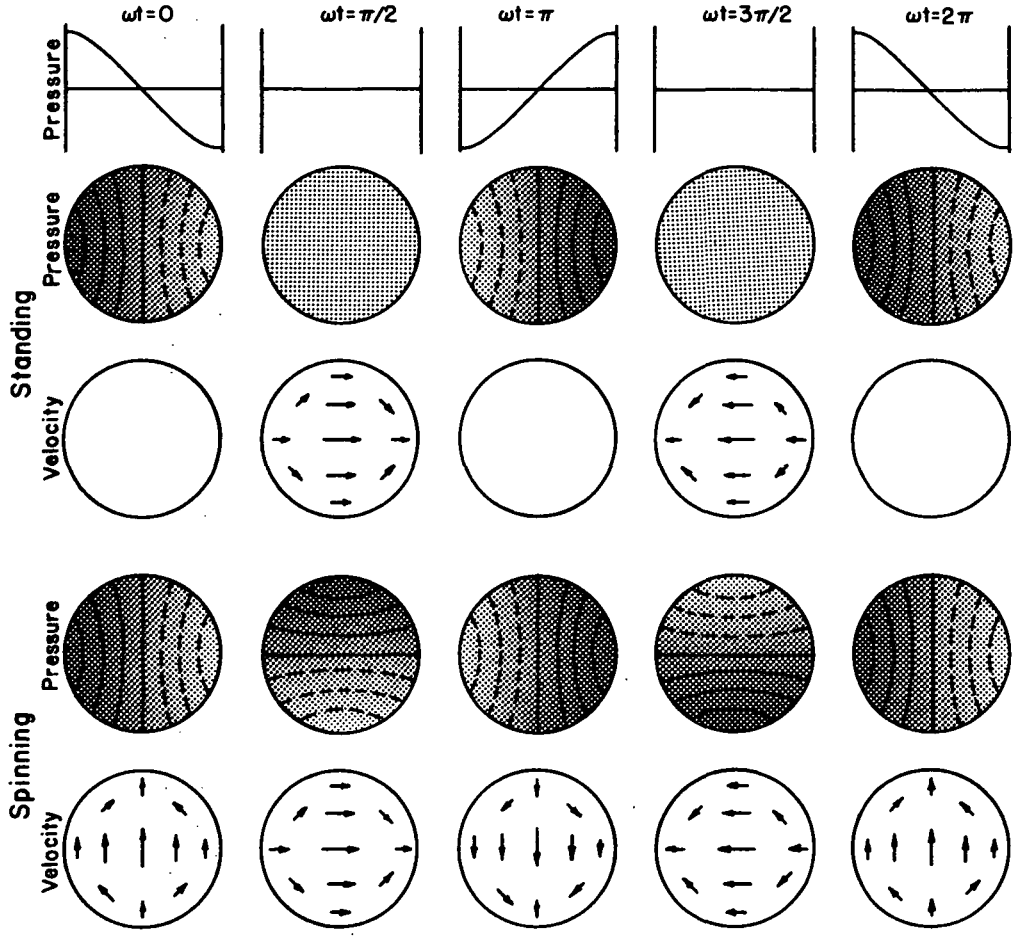

Figure 2. Comparison of Standing and Spinning <100> (First Tangential) Modes of Vibration

Therefore, for the summation of <100> and <202> vibrations,

$$P' = P'_{100} + P'_{202}$$

$$= \tilde{P}'_{100} \cos(\omega_{100}t) + \tilde{P}'_{202} \cos(2\omega_{100}t + \frac{\pi}{2} - \phi)$$

$$= \tilde{P}'_{100} [\cos(\omega_{100}t) + P_{21} \cos(2\omega_{100}t + \frac{\pi}{2} - \phi)] \qquad (18)$$

where P_{21}, the amplitude ratio of the acoustic pressure components at that location, is

$$P_{21} = \tilde{P}'_{202}/\tilde{P}'_{100} \qquad (19)$$

and the angle ϕ is the relative phase between the two components.

To determine the output of the CTHWA's response to specific acoustic oscillations, the hot wire must first be calibrated to determine the constants A and B and the exponent m used in equations (5), (6) and (7). Details of this procedure are given by Fang and Purdy [8]. The exponent m was found to be 0.444. Once the wire is calibrated, the equations for the acoustic oscillations can be substituted into the CTHWA equation, equation (9), to obtain the corresponding anemometer output.

Equation (9) is nonlinear. The term $|\vec{V}|$, which is part of the Reynolds number, rectifies the velocity; this strongly effects the frequency components of the output of the CTHWA. Also, $|\vec{V}|$ only consists of velocity components normal to the hot wire since the hot wire is not sensitive to a velocity component parallel to its axis.

In a liquid-propellant rocket engine, the burning rate is

composed of a time-mean and a fluctuating component, $W = \overline{W} + W'$. It is the energy release associated with W' which produces gas oscillations. In the analog system, E^2 is proportional to the energy release rate from the hot wire to the gas of the system. E^2 can also be considered to be the sum of a time-mean and a fluctuating component, $E^2 = (\overline{E^2}) + (E^2)'$. It is the energy release associated with $(E^2)'$ which produces gas oscillations. Fang [3] has shown that, in the range of voltages of interest, $(E^2)'$ is adequately represented by E'. Since the output of the anemometer is E', E' rather than $(E^2)'$ was used in the research.

It is important to know the characteristics of E' when acoustic oscillations—similar to those which occur during unstable combustion—are imposed on the hot-wire. The characteristics of importance are the resulting frequency components, the relative magnitudes of these components and how the relative magnitude of the components are effected by changing the ratio P_{21} and the phase angle ϕ. To obtain this information, a fourier series analysis was done on the fluctuating component of the CTHWA output E' when perturbed by a variety of sinusoidal and distorted sinusoidal inputs. The fourier coefficients which result from the analysis of E' will be presented later. The results will then be compared to the characteristics of the chamber and the interaction of the two discussed.

APPARATUS AND EXPERIMENTAL INVESTIGATIONS

Introduction

Experimentally, two types of closed-loop situations were investigated—one used a microphone in the feedback system, the other used the CTHWA in the feedback system. The microphone system is a

relatively simple linear feedback system. The output of the microphone, when excited by a pressure perturbation, is an electrical signal having virtually the same frequency components and waveform as the perturbing signal. The CTHWA system is a nonlinear feedback system. If the hot-wire transducer is exposed to an unsteady velocity field composed of one frequency component, the CTHWA's output signal is predominantly composed of a component at twice that frequency, with lesser components at the original frequency and at the higher harmonic frequencies. The anemometer output signal E' is not linearly related to the unsteady velocity components being sensed.

The main purpose of the research was to investigate the CTHWA closed-loop performance. The linear microphone system was investigated to determine the characteristics of the chamber and the electronic equipment, and to establish the conditions necessary for self-sustenance of a closed-loop system.

Apparatus

The test chamber used in all the experiments was an aluminum cylinder with 0.0254-meter-thick walls and plexiglass end plates. The inside of the chamber was 0.2049 m in diameter and 0.3130 m long. On one end-plate there was provision for mounting several acoustic drivers; however, only one driver was used. In the same end plate, there were three holes in which microphones could be placed so that they were flush with the inside surface. In addition to the end-plate microphones, there was also a microphone located in the cylinder wall 0.0173 m from the end of the chamber. Also, the probe holder of the CTHWA could be inserted through an additional access hole in the cylinder wall

so that the hot wire itself could be located in the same transverse plane as the microphone—0.0173 m from the end plate containing the acoustic driver. The hot wire was directly under the microphone. The radial location of the hot wire was adjustable.

The acoustic driver was mounted on the end plate with the "top" of its opening tangent to the inside surface of the cylinder. The end plate could be rotated to obtain any angular position of the driver relative to the microphone and hot wire. For the microphone closed-loop experiments, the driver was at the same angular position as the microphone mounted in the cylinder wall. For the CTHWA closed-loop experiments, the driver was located at 225 degrees with respect to this microphone. Figures 3 and 4 are photographs of the test chamber and the electronic equipment, respectively.

Figure 5 is a schematic of the closed-loop microphone system. Before carrying out the closed-loop investigations, the resonant frequencies of the chamber were determined and the phase characteristics of each piece of equipment were measured. Of special importance in this work is the relative phases of all frequency components of all signals involved. Phase relationships strongly effect whether signals add constuctively or destructively. Because of this, the amount of phase change, as a function of frequency, through each component of the system, was measured. Phase changes can be considered to be the sum of two components—time delay and phase shift. Except for the time-delay tape recorder, the two components were not separately measured. Only the net phase change was established; i.e., if a signal was time delayed by two and a half cycles, the measured phase change would be

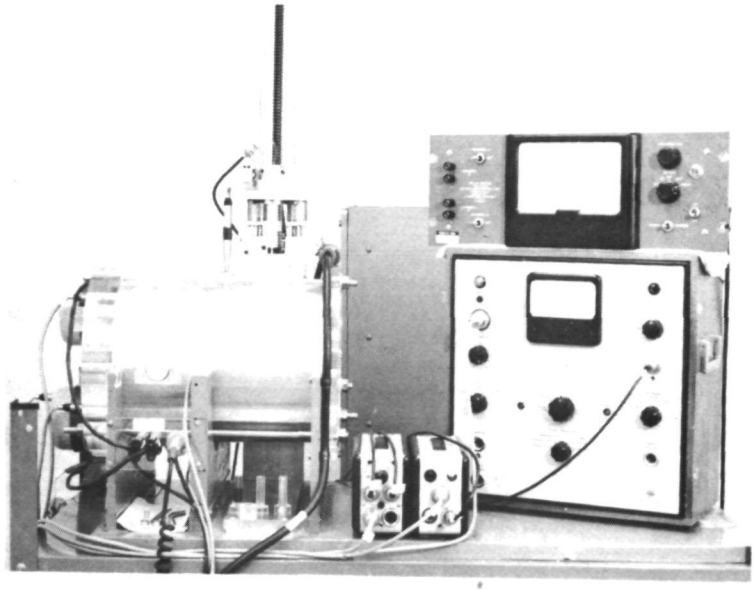

Figure 3. Photograph of the Test Chamber

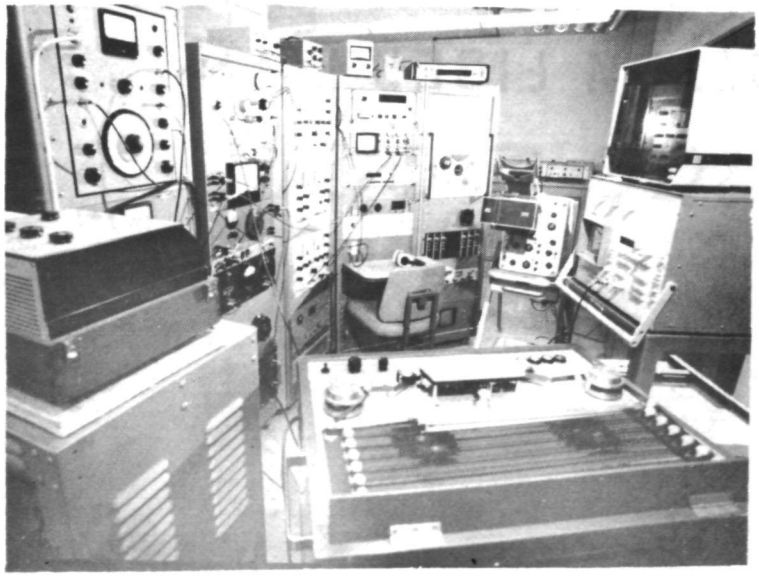

Figure 4. Overview of the Electronic Equipment

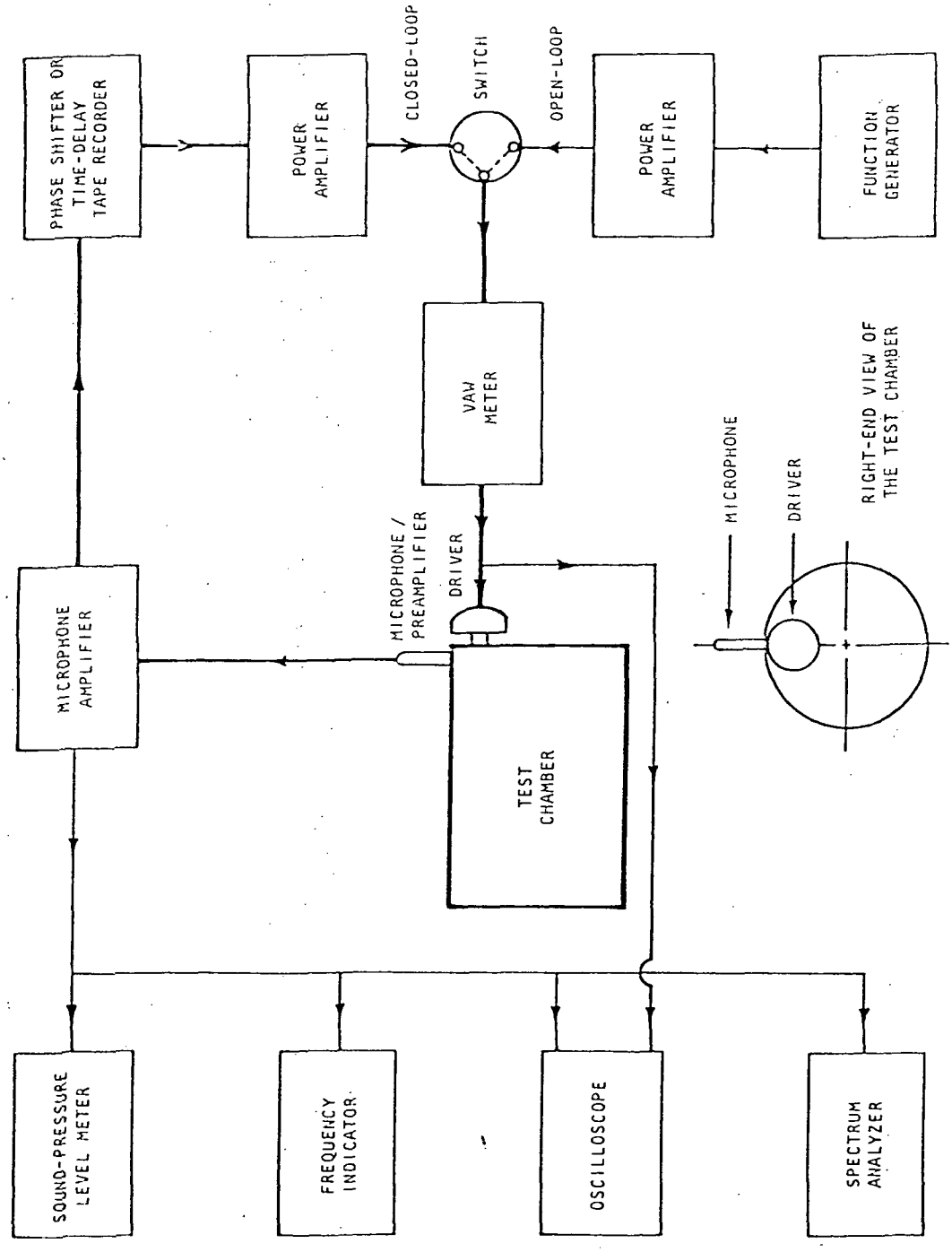

Figure 5. Schematic Diagram of the Microphone Closed-Loop Experimental System

180 degrees, not 900 degrees.

As can be seen in Figure 5, two phase-change devices were used in the experiments—a phase shifter and a time-delay tape recorder. The phase shifter changed the phase of each frequency component of a signal passing through it by an amount determined by the dial setting, plus an additional amount which depended upon the frequency of the component. Because of this, when a multifrequency signal passed through the phase shifter, its waveform was altered—the amplitude of each frequency component remained the same, but the phase relationships between components changed.

A similar process occurred through the time-delay tape recorder—there was a fixed amount of phase shift through the recorder (not a function of frequency), plus an additional phase shift which depended on frequency (fixed time-delay period), plus the amount of phase shift associated with the time-delay dial setting (variable time-delay period).

MICROPHONE EXPERIMENTS

The closed-loop microphone feedback system in Figure 5 can initially be excited by an energized signal from a function generator or a white-noise generator—open-loop excitation—or system electronic noise—closed-loop excitation. The energized signal excites the acoustic driver, which generates an acoustic field in the chamber. The microphone senses the acoustic pressure fluctuations of the acoustic field and converts its diaphragm vibrations into an electrical signal by means of a microphone preamplifier and amplifier. The amplified microphone signal can then either be phase shifted or time delayed, energized and, when the switch is moved to the closed-loop position, sent to the

acoustic driver where it becomes the source of acoustic energy in the chamber.

The object was to study the evolution of the acoustic field after the loop was closed; i.e., to determine: if the acoustic pressure disturbance would decrease in level, increase in level, oscillate in level, die out or reach some steady-state level; if the frequency components of the acoustic pressure would remain the same or change to some other frequency components; and the minimum energization and the phase change necessary to have steady-state operation after the loop is closed.

The procedures used were as follows:

- The chamber was acoustically excited using the open-loop mode of operation with the function generator or white-noise generator acting as the signal source.
- The system was allowed to run open-loop long enough for steady-state conditions to be established. Meanwhile, the amount of phase change and energization in the feedback loop were adjusted to the desired values.
- The loop was then closed and the results observed. If the acoustic field in the chamber died out, the system was switched back to the open-loop condition and the energization provided by the feedback-loop amplifier was increased. The loop was then closed again and the results observed. This procedure was continued until the minimum power to obtain sustained closed-loop operation was determined. Likewise, if there was too much energization in the closed-loop so that the acoustic pressure kept increasing in level, or was

self-sustained at a level higher than the minimum level, the energization was reduced until the minimum level required to maintain steady-state closed-loop operation was established. The power to the driver was then the minimum power required for self-sustenance of the sound field at a given amount of phase change. A record was kept of the properties of the initiating signal, the amount of phase change, the power to the driver and the resulting frequency(ies) of the sound field(s) during closed-loop steady-state minimum power operation.

- The amount of phase change was altered and the foregoing procedures were repeated until the desired range of phase change was covered.

A variation of the above procedure was to fix the loop gain and vary the phase change to determine the frequency(ies) and sound pressure level of the resultant acoustic field(s), as a function of phase change.

HOT-WIRE EXPERIMENTS

The closed-loop CTHWA feedback system is shown in Figure 6. It is similar to the microphone closed-loop system; however, the acoustic driver is now 225 degrees from the top of the chamber, 225 degrees from the hot wire and 180 degrees from a microphone located in the endplate. (The location of the acoustic driver relative to the hot wire was so chosen to avoid locating the hot wire at a velocity node.) Also, this system had a preamplifier just before the power amplifier to obtain finer control of the loop gain.

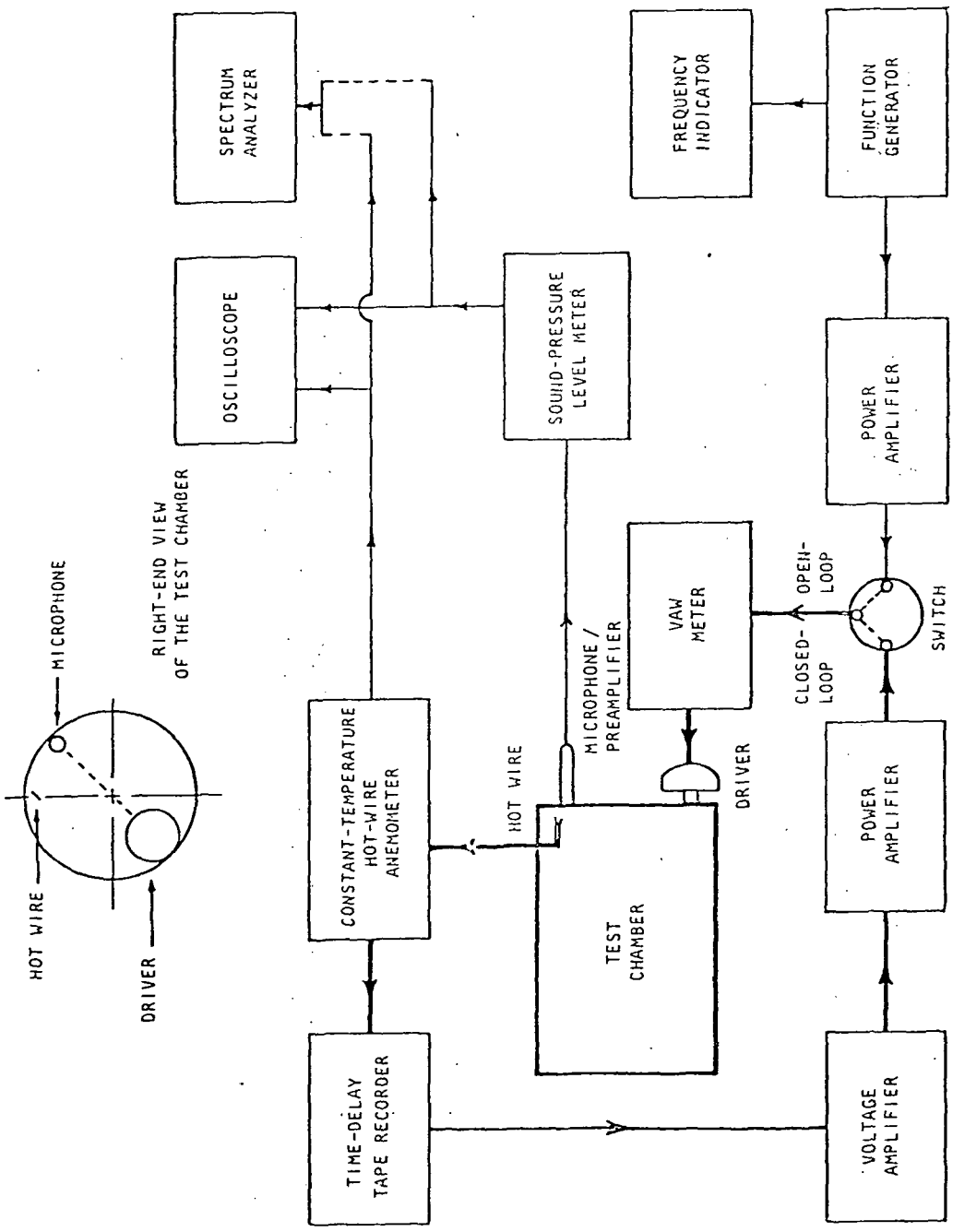

Figure 6. Schematic Diagram of the CTHWA Closed-Loop Experimental System

ANALYTICAL RESULTS

A fourier analysis of the CTHWA output signal, resulting from the exposure of the hot wire to several different acoustic fields, was performed. Figure 7 shows P', E' and the magnitude of the fourier coefficients of E' for a <100> sound field. The odd harmonic coefficients are smaller than the even ones and the second harmonic component (the component whose frequency is twice f_{100}) is dominant.

Adding a <202> sound field to the <100> sound field changes the relative magnitudes of the frequency components. Figure 8 shows P', E' and the magnitude of the fourier coefficients of E' for a <100> plus <202> sound field when $P_{21} = 0.5$ and the phase angle $\phi = 90$ degrees. Note that adding the <202> sound field significantly increased the magnitude of the component at the fundamental frequency.

Figure 9 examines more closely the effect of P_{21} on the first two harmonic components of E'. Adding even a weak <202> sound field to the <100> sound field increases the magnitude of the fundamental frequency component significantly.

EXPERIMENTAL RESULTS

Calibrations

The phase change through the phase shifter ψ_{PS}, in degrees, was found to be composed of two components—ψ_{ZS}, the zero-phase-shift dial setting which was a function of the signal frequency, and ψ_{DIAL}, the dial setting—such that

$$\psi_{PS} = \psi_{ZS} - \psi_{DIAL} \tag{20}$$

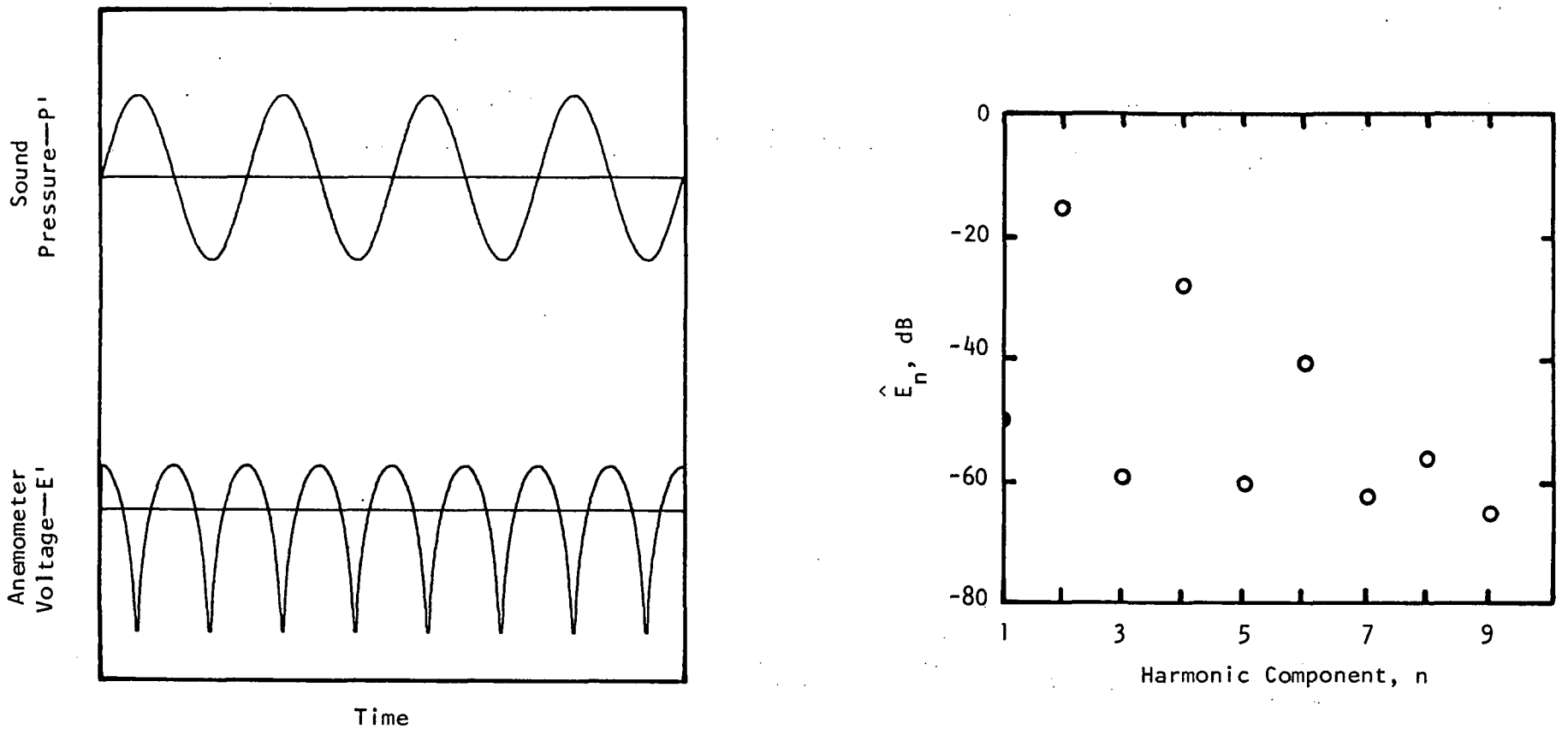

Figure 7. Analytically Predicted Acoustic Pressure P', CTHWA Output Signal E' and Fourier Analysis of E' for a <100> Sound Field with L_p = 144.8 dB

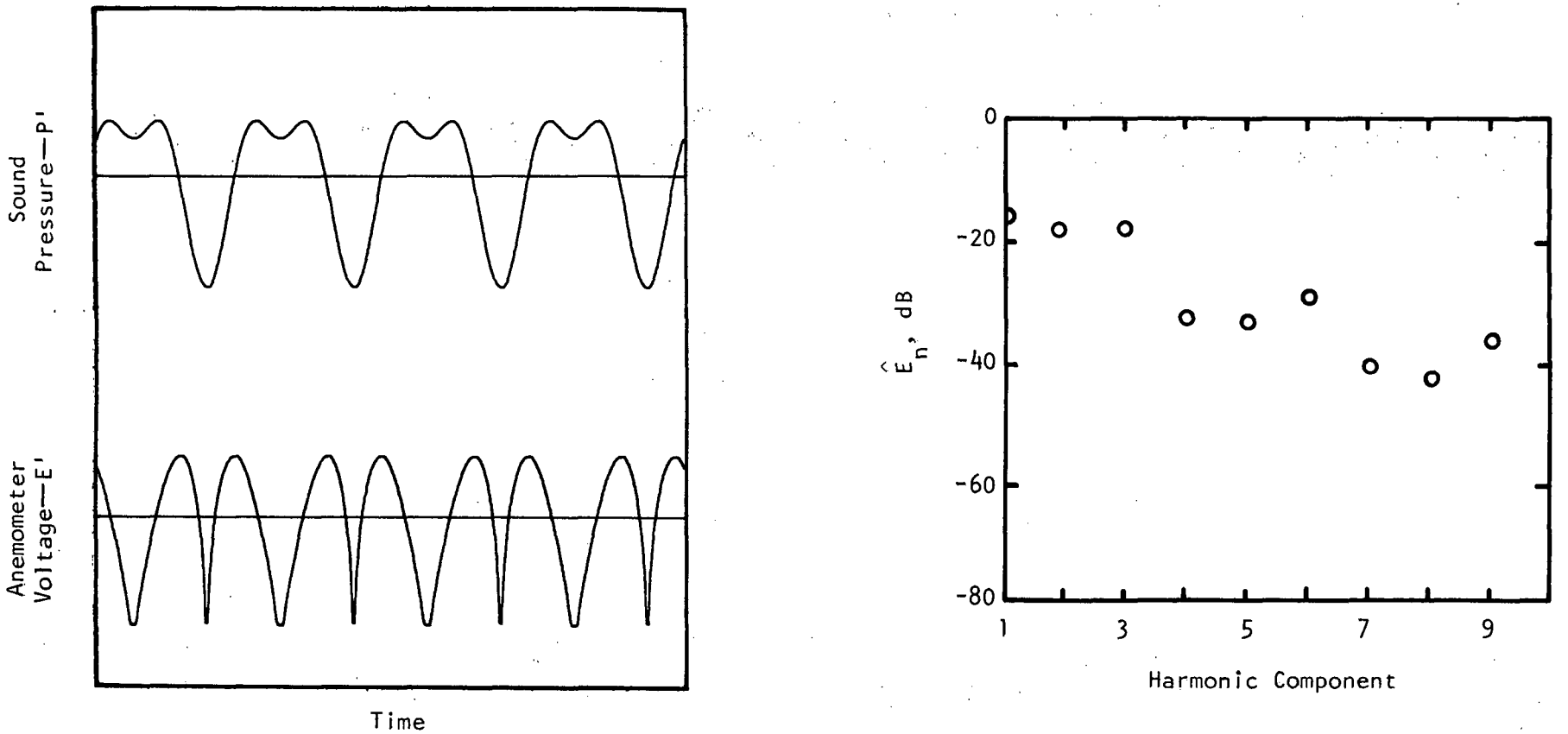

Figure 8. Analytically Predicted Acoustic Pressure P', CTHWA Output Signal E' and Fourier Analysis of E' for <100> + <202> Sound Field with $P_{21} = 0.5$, $\phi = 90^0$ and $L_p = 144.8$ dB

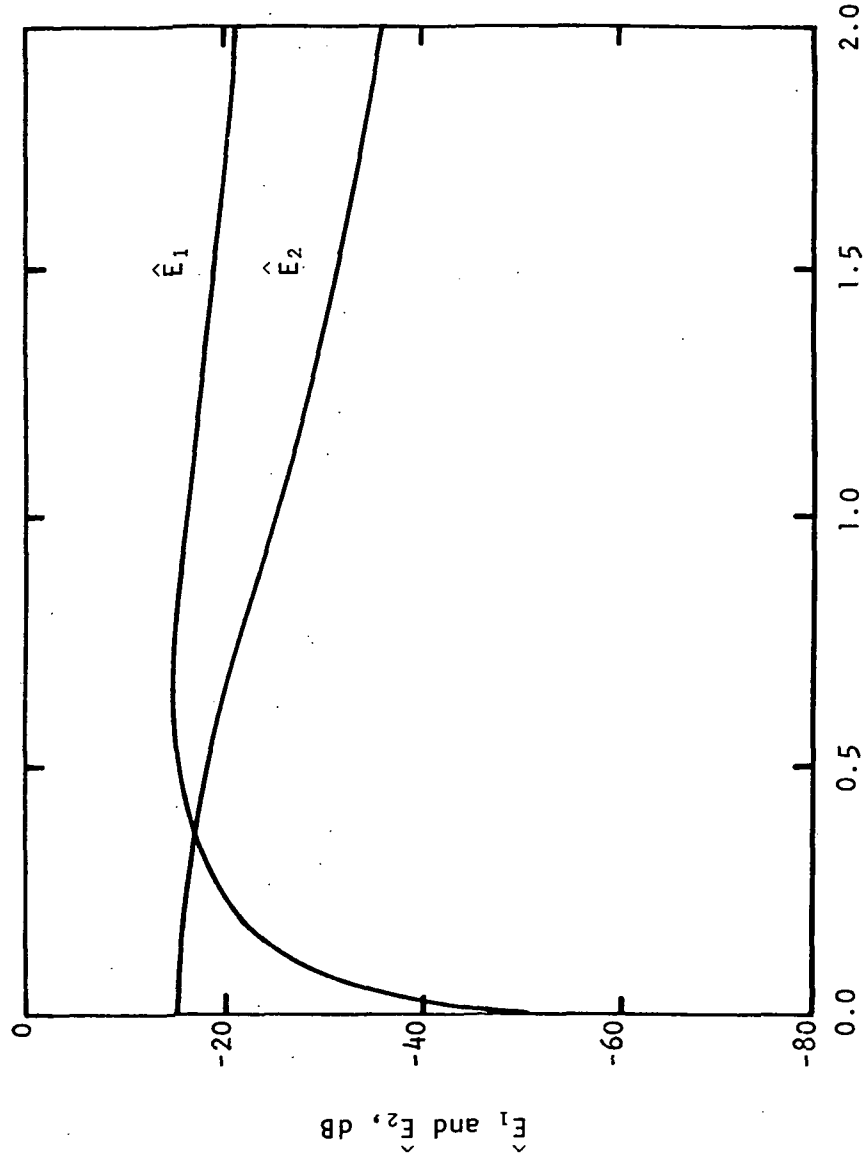

Figure 9. Variation of the First Two Harmonic Components of the Analytically Predicted CTHWA Output Signal E' with P_{21} for $\phi = 90^0$ and $L_p = 144.8$ dB

Table 1 lists values of ψ_{ZS} for selected resonant-mode frequencies. These data, plus others, were used to determine the following empirical equation for ψ_{ZS}:

$$\psi_{ZS} = 63.79 \ln(f/40) \tag{21}$$

where f is the signal frequency in hertz and ψ_{ZS} is in degrees. This phase shift is equivalent to a time delay, in seconds, of

$$\psi_{PS} = \psi_{PS}/360 \ f \tag{22}$$

Table 1. Values of ψ_{ZS} and $\psi_{P/D}$ at Selected Frequencies

f (Hz)	Mode $\langle mnn_z \rangle$	ψ_{ZS} (degrees)	$\psi_{P/D}$ (degrees)	
			Fig. 4	Fig. 5
992.5	100	201.6	279.2	105
1107.0	002	207.5	289.1	
1493.5	102	223.7	34.6	
1740.5	201	232.6	91.6	
1985.0	202			105
2326.5	301	254.3	109.3	

The time delay, in seconds, through the time-delay tape recorder, as a function of frequency f, in hertz, and dial setting R, is

$$\tau_{C7} = 0.02200 - 0.5417/f + (R - 215)/148,000 \tag{23}$$

This is equivalent to a phase change, in degrees, of

$$\psi_{C7} = 7.920\ f - 195 + (R - 215)f/411.1 \qquad (24)$$

The phase change through the power amplifier ψ_{PA} in the closed-loop circuit was zero.

An equation for the phase change between the input to the acoustic driver and the output of the microphone amplifier $\psi_{P/D}$ was not obtained, but it was a function of frequency. The phase changes for the microphone and the CTHWA closed-loop systems, are also given in Table 1. The values of $\psi_{P/D}$ were different because the location of the microphone with respect to the driver was different for the two closed-loop systems.

The phase change through the CTHWA, $\psi_{E/P}$, was measured with respect to the microphone amplifier output; however, there was considerable scatter in these data so the values were considered to be approximations only. The approximate value of $\psi_{E/P}$ for 992.5 Hz was minus 90 degrees and at 2261.0 Hz it was plus 90 degrees. The phase change ψ_{VA} through the voltage amplifier in the CTHWA closed-loop was zero for all frequencies.

The resonant frequencies of the chamber were determined. Figure 10 is a spectrum analysis of the microphone amplifier output in response to the chamber being excited by white noise. The resonant frequencies are identified, along with their mode numbers. Note that $f_{202} = 2f_{100}$. In checking the resonant frequencies of the chamber, data were taken on the power input to the driver necessary to generate a resonant acoustic field of a particular sound-pressure level (L_p = 150.0 dB). The data are presented in Table 2 in the order of increasing power required.

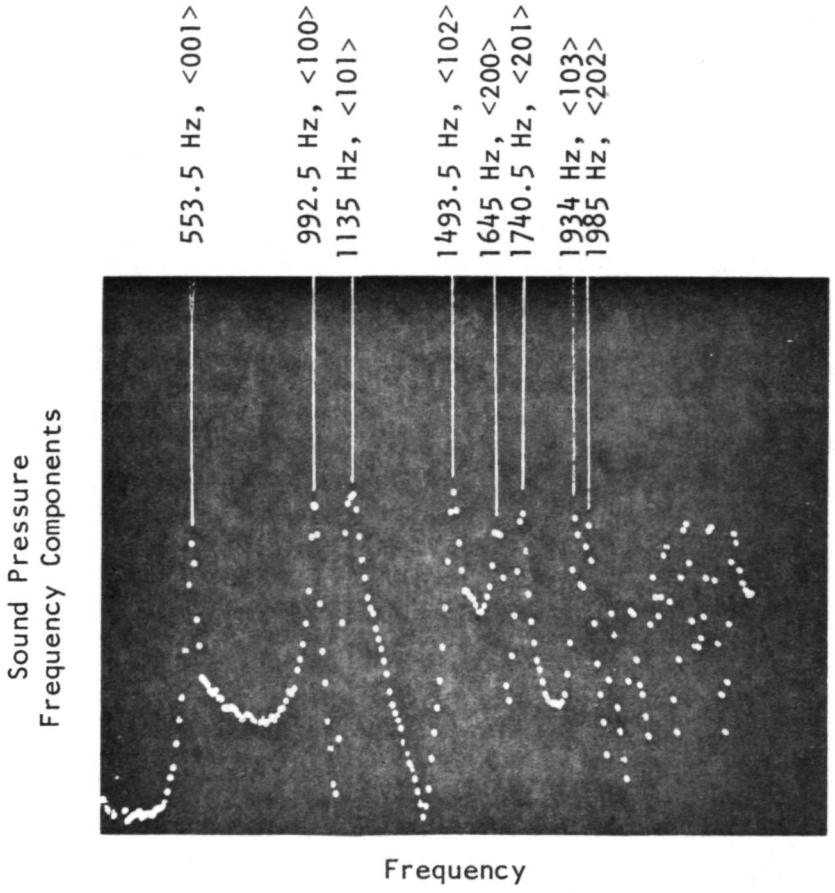

Figure 10. Spectrum Analysis of the Microphone Output in Response to the Chamber Being Excited by White Noise

Table 2. Power Required to Generate Resonant Acoustic Fields for which L_p = 150.0 dB

f (Hz)	Mode $\langle mnn_z \rangle$	Power (watts)
996	100	0.34
1108	002	0.36
2329	301	0.46
1138	101	0.47
1742	201	0.72
1496	102	0.74
1941	103	0.89
1654	200	0.99
2267	300	1.07
2512	302	1.48
2341	203	1.84
2427	104	1.93
1992	202	2.04

Microphone Closed-Loop System

In the microphone feedback closed-loop experiments, it was found that the resultant acoustic field during closed-loop operation did not depend in any way on the initiating acoustic field. Figure 11(a) is a multiple-exposure photographic record of the oscilloscope display of the output of the microphone amplifier as the system is changed from the open-loop to the closed-loop mode of operation. The initiating acoustic field was a <100> sound field having a frequency of 992.5 Hz; the phase shifter—set at $\phi_{DIAL} = 0^0$—was used as the phase change

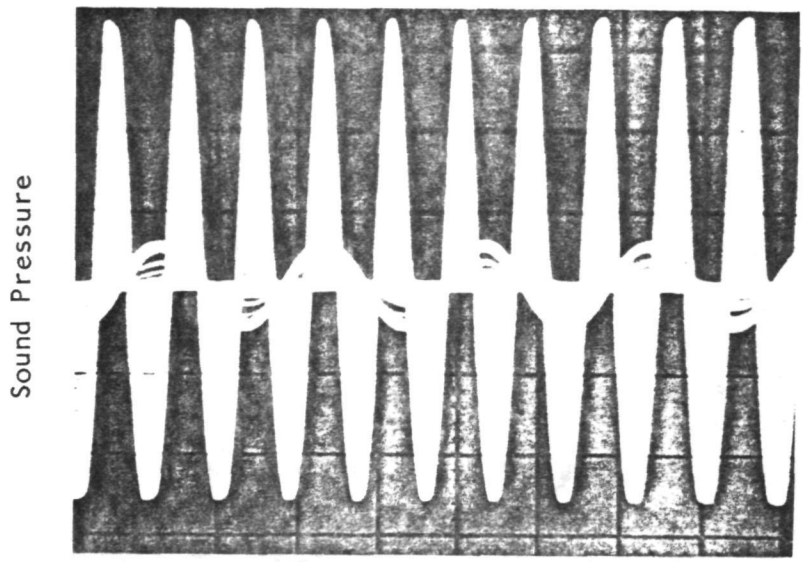

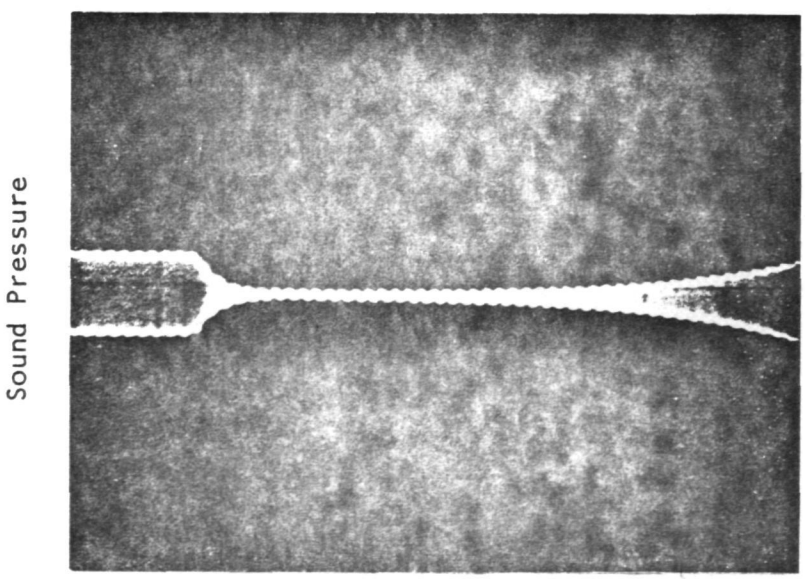

Figure 11. Behavior of the Acoustic Pressure During Transition from Open-Loop to Microphone Closed-Loop Operation—Open-Loop Acoustic Field = <100>; $\psi_{DIAL} = 0^0$; $T = 26^0C$; Resulting Closed-Loop Acoustic Field = <301>

device. When the loop was closed, the <100> sound field died out and a <301> sound field (f_{301} = 2326.5 Hz) developed. Another view of the same phenomena is shown in figure 11(b) where the time history of the acoustic pressure is shown before and after the time when the loop was closed. At the left is the initial open-loop signal at f_{100} = 992.5 Hz. When the loop was closed, the <100> sound field died out and the <301> sound field developed.

Changing the initiating acoustic field, while leaving everything else the same, yielded the same results. Figures 12(a) and 12(b) are oscilloscope photographs obtained when the initiating field came from low-level electronic noise in the feedback loop, rather than the <100> sound field. Although the initial situation is different than that in Figures 11(a) and 11(b), the resultant acoustic field is the same.

Eventually both of the above cases reached a steady-state level. Figure 13 has a longer sweep time and shows the entire development of the acoustic field from that produced by electronic noise to the steady-state <301> sound field.

A single resonant-frequency acoustic field did not always result during closed-loop operation; sometimes acoustic pressure fields with two or more frequency components developed. Figure 14(a) is the microphone output (upper trace) and signal to the driver (lower trace) during steady-state closed-loop operation, with the phase shifter dial set at 140 degrees. Figure 14(b)—a spectrum analysis of the microphone amplifier output—shows the acoustic field to be primarily the summation of <100> and <002> resonant sound fields.

Figure 15 shows the results obtained from the microphone closed-loop system, using the phase shifter as the phase-change device, for

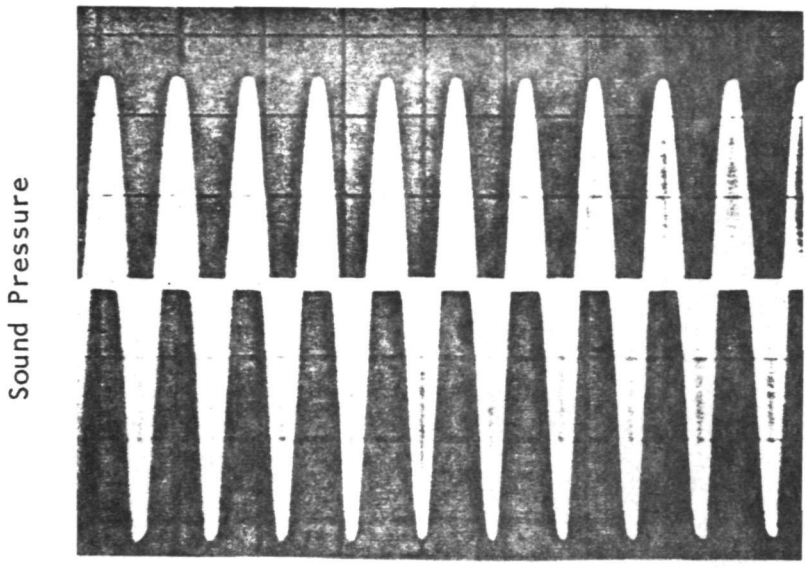

(a)

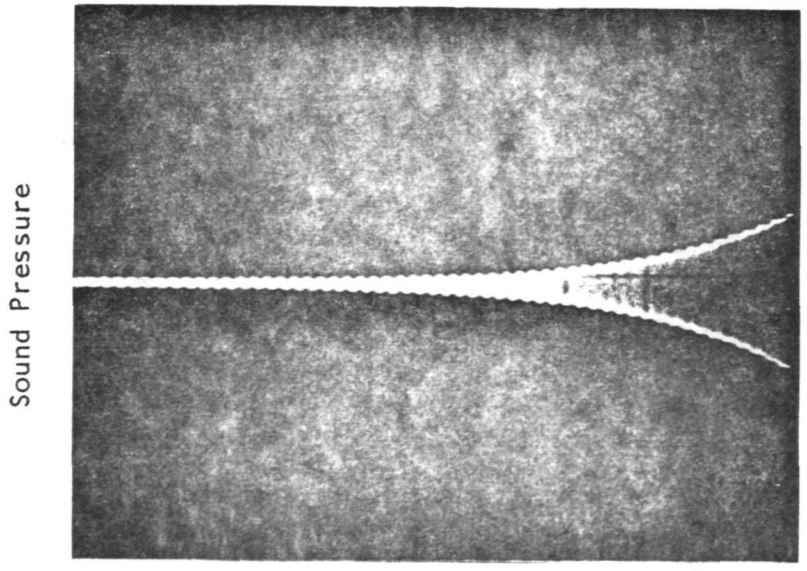

(b)

Figure 12. Behavior of the Acoustic Pressure During Transition from Open-Loop to Microphone Closed-Loop Operation—Initial Acoustic Field from Electronic Noise; $\psi_{DIAL} = 0^0$; $T = 26^0C$; Resulting Closed-Loop Acoustic Field = <301>

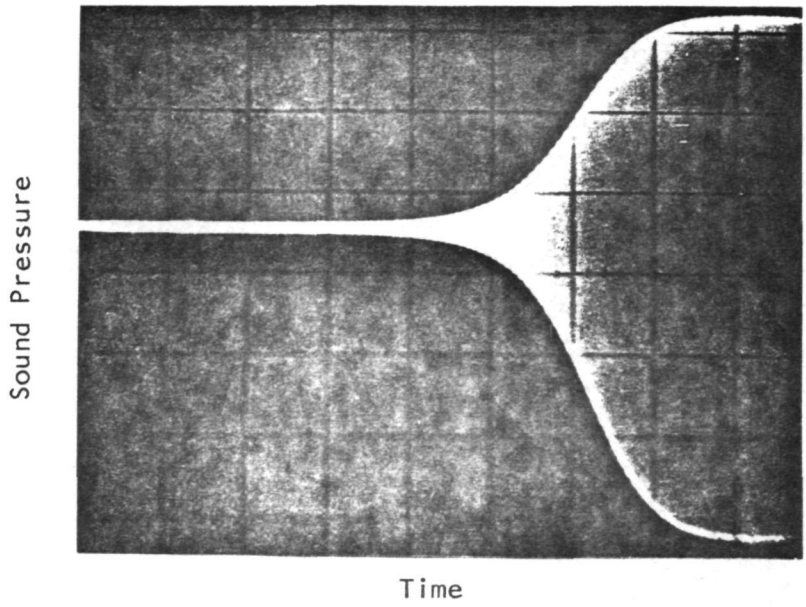

Figure 13. Behavior of the Acoustic Pressure During Transition from Open-Loop to Microphone Steady-State Closed-Loop Operation— Initial Acoustic Field from Electronic Noise; $\psi_{DIAL} = 0^0$; $T = 26^0C$; Resulting Closed-Loop Acoustic Field = <301>

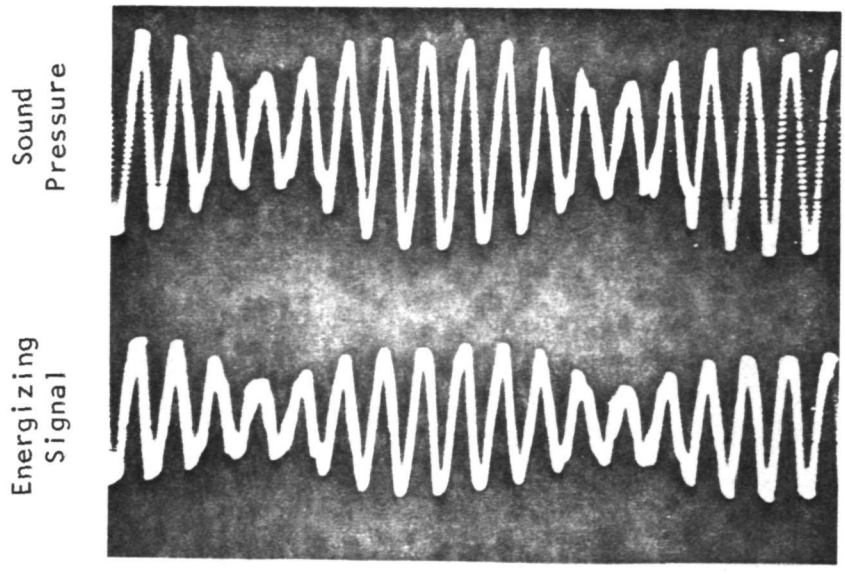

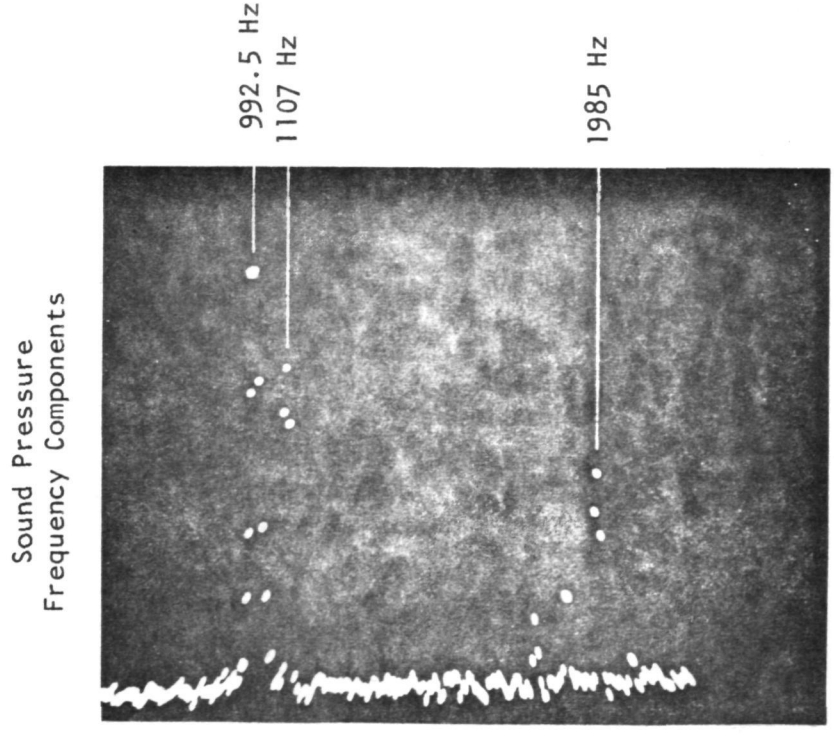

Figure 14. Resultant Sound Field of Microphone Closed-Loop Operation—T = 26°C and $\psi_{DIAL} = 140^{\circ}$

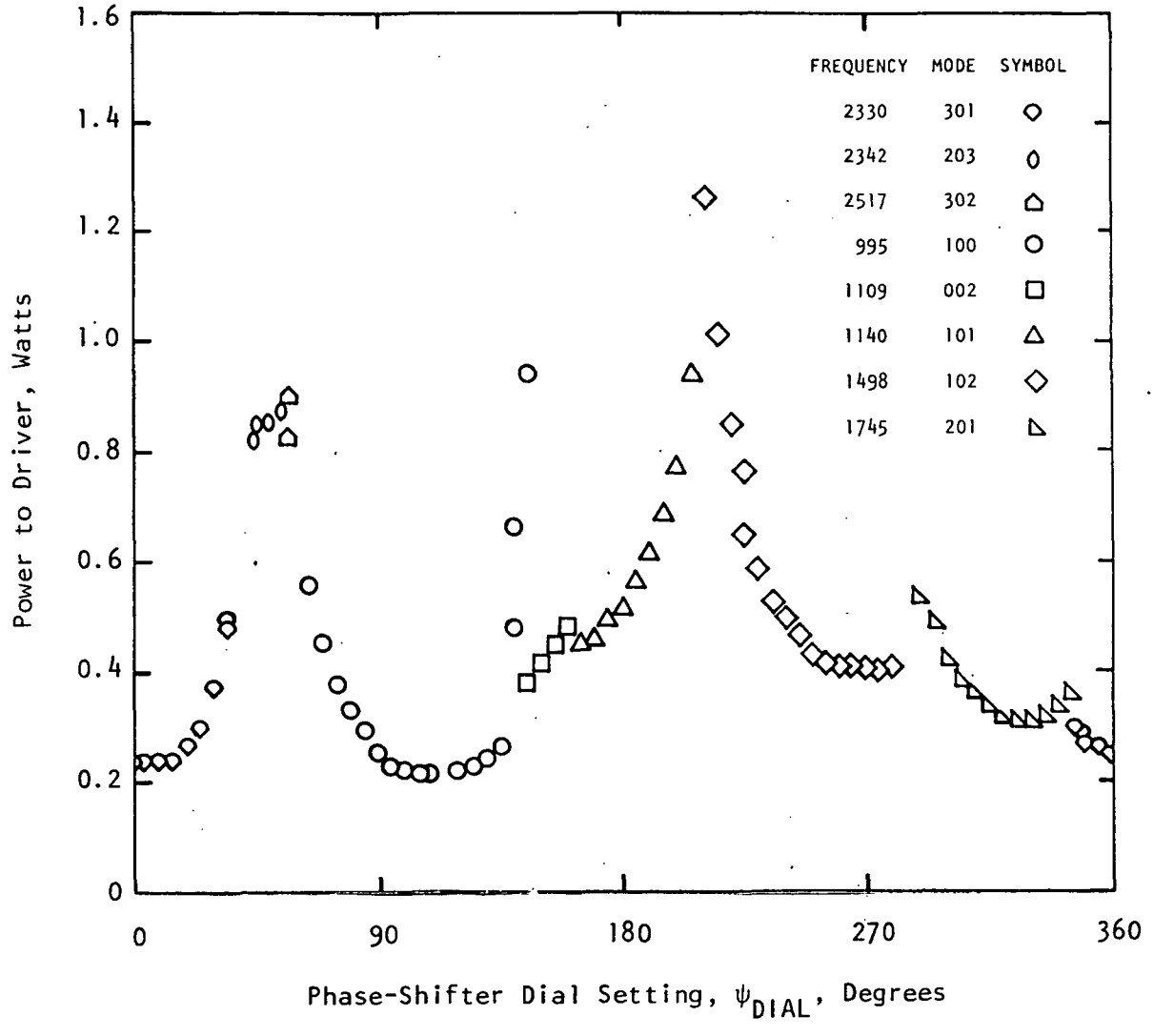

Figure 15. Closed-Loop Acoustic Field(s) and Power Required for L_p = 150.0 dB for Various Phase-Shifter Dial Settings

various phase shifter dial settings. For each dial setting, the resulting acoustic field(s) was(were) determined and the driver power required to maintain a sound pressure level of 150.0 dB was established. When the gain in the loop was increased for a given phase-shifter dial setting, a steady-state situation could still be attained, but the resulting sound pressure level would increase. Results similar in character to the above were also obtained using the time-delay tape recorder as the phase change device.

So far, all the phase shifts and time delays have been recorded as dial settings. These can be converted to actual phase shifts through the entire closed-loop using the calibration information given earlier. Referring to figure 5, the total time delay through the microphone closed-loop was

$$\psi_{TOTAL} = [\psi_{P/D} + (\psi_{PS} \text{ or } \psi_{C7}) + \psi_{PA}] - 360\ n \qquad (25)$$

(The purpose of the last term was to reduce ψ_{TOTAL} to a value between 0 and 360 degrees). Using equation (25), ψ_{TOTAL} was calculated for the resulting acoustic fields in the cases previously presented.

In Figure 11 the initiating sound field was a <100> one at a frequency of 992.5 Hz, and the total phase change through the loop ψ_{TOTAL} was 121 degrees. When the microphone signal was fed back to the driver it was out of phase with the existing acoustic oscillation; hence, the <100> sound field died out. The resulting steady-state sound field was the <301> one at a frequency of 2326.5 Hz, and its total phase change through the loop was four degrees—the acoustic oscillation generated by the driver was almost in phase with the existing acoustic oscillation in the chamber. When the loop was closed,

the system transitioned from the <100> sound field to a <301> sound field. For the <301> sound field the existing and feedback acoustic oscillations were approximately in phase, thereby adding as constructively as possible.

In Figure 12 the same phenomena occurred; the system selected, from the acoustic field produced by the electronic noise in the system, that frequency for which the existing and feedback acoustic oscillations were approximately in phase. The value of ψ_{TOTAL} for the <301> sound field was again four degrees.

At some phase-shifter settings there were no frequencies for which ψ_{TOTAL} was about zero. There the system selected the frequency or frequencies for which the ψ_{TOTAL}'s deviated somewhat from zero.

The driver power required to produce a sound field of a given frequency also affected the resultant acoustic field. In figure 14, a <100> sound field with a ψ_{TOTAL} of 341 degrees in the feedback loop and a <002> sound field with a 357-degree phase change in the feedback loop both developed. Although the <002> sound field has a phase change closer to zero, the <100> sound field was dominant because it was easier to drive. (Table 2 lists acoustic fields in ascending order of relative power required to drive each.)

If figure 15 each optimum phase shifter setting occurred at a value for which ψ_{TOTAL} was approximately zero degrees. This is clearly illustrated by figure 16 which recasts the data of figure 15 in terms of ψ_{TOTAL} instead of ψ_{DIAL}.

In summary, the microphone closed-loop experiments showed that self-sustenance could always be attained if the energization in the loop was great enough. The amount of energization needed was related

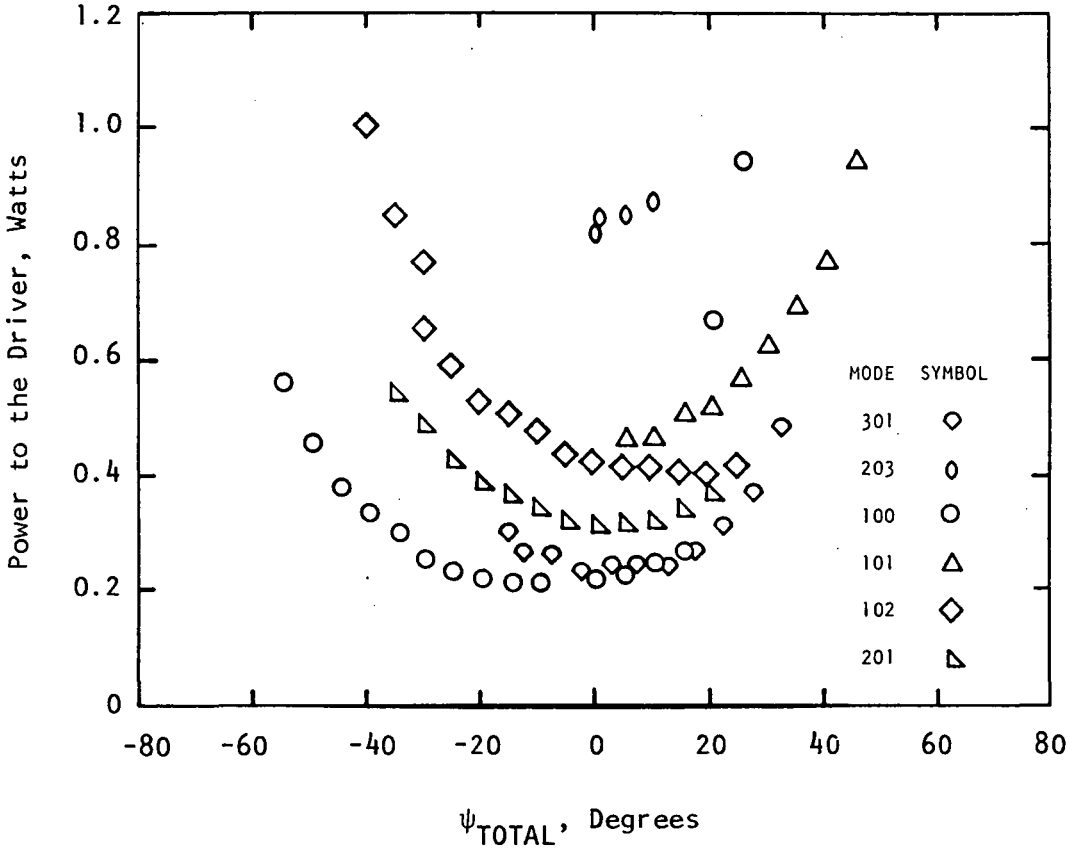

Figure 16. Closed-Loop Acoustic Fields and Power Required for L_p = 150.0 dB in Terms of ψ_{TOTAL}

to the deviation of ψ_{TOTAL} from zero degrees and the relative amount of energization needed to drive the acoustic field of interest. More than one frequency could result if conditions were suitable for both. The resulting frequencies were always resonant frequencies. They did not depend upon the initial open-loop frequency, but upon ψ_{TOTAL}, the total phase change through the loop for the frequencies of interest. The closer the total phase change for a particular frequency was to a complete cycle, the easier it was to sustain that frequency. In short, Rayleigh's criterion [4] was the dominant factor controlling the response of the microphone (linearly pressure sensitive) system during closed-loop operation.

CTHWA Closed-Loop

Figure 17 illustrates a typical transition from open-loop to self-sustained closed-loop operation using the CTHWA output as the feedback signal. The figure is a long time-base oscilloscope display of the sound pressure and CTHWA output voltage, starting just prior to closing the loop and ending with the steady-state, closed-loop operation. The open-loop acoustic field was <100> at 991.5 Hz; the steady-state closed-loop acoustic field was primarily <100> at 991.5 Hz plus <202> at 1983.0 Hz. Figure 18 is an oscilloscope record of the same phenomena, but having a shorter time base so that the wave forms could be seen. In the upper part of the figure, the open-loop sound pressure and the closed-loop steady-state pressure were superimposed; likewise, in the bottom part the open-loop and closed-loop CTHWA outputs were superimposed.

Changing the open-loop initiating signal did not change the frequencies which developed when the loop was closed. At the same

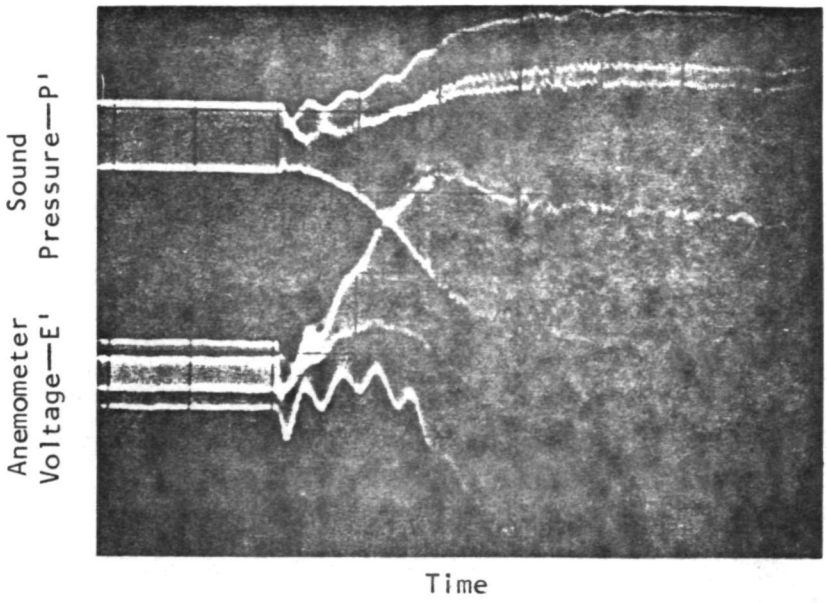

Figure 17. Transition from Open-Loop to Self-Sustained Steady-State Closed-Loop Operation—T = 26°C; R = 260; Initial Acoustic Field = <100>; Resulting Closed-Loop Acoustic Field = <100> + <202>

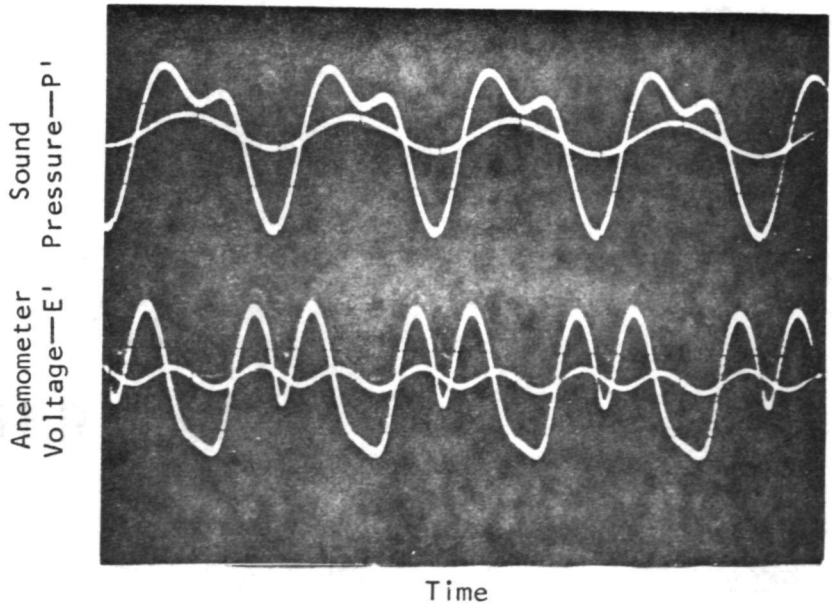

Figure 18. Open-Loop and Self-Sustained Steady-State Closed-Loop Microphone and CTHWA Outputs—T = 26°C; R = 260; Initial Acoustic Field = <100>; Resulting Closed-Loop Acoustic Field = <100> + <202>

time delay setting of R = 260.0, a white noise signal and the electronic noise in the system were each used as the initiating signal. Both resulted in the <100> plus <202> sound field; however, more gain was required in the loop to initiate self-sustenance for these two cases. (The stability of this system appears to be dependent upon the nature of the perturbation sound field; this phenomenon will be quantitatively investigated in a future study.)

Figure 19 is a map of the minimum feedback-loop gain required to initiate self-sustenance for various amounts of time delay through the tape recorder. An initiating <100> sound field at a frequency of 991.5 Hz and a sound-pressure level of 153.8 dB was used. Whenever the gain was equal to or greater than that shown in the figure for a particular setting, closed-loop operation would be self-sustaining; whenever the gain was less than that shown in the figure for a particular setting, closed-loop operation would not be self-sustaining. It was possible to initiate self-sustenance at any time-delay setting, provided there was sufficient gain in the loop.

In figure 19, three different self-sustained acoustic fields are depicted: one steady in waveform and level having frequency components at f_{100}, f_{202} ($f_{202} = 2f_{100}$) and their higher harmonics; one unsteady in waveform and level having frequency components at f_{100}, f_{202} and their higher harmonics; and one transitional in waveform and level having frequency components at f_{100}, f_{202} and their higher harmonics and f_{101}, f_{300} ($f_{300} \approx 2f_{101}$) and their higher harmonics. Figures 20, 21 and 22 illustrate the characteristics of each of the above types of self-sustained acoustic field. The reasons for the different types of closed-loop acoustic field were determined from

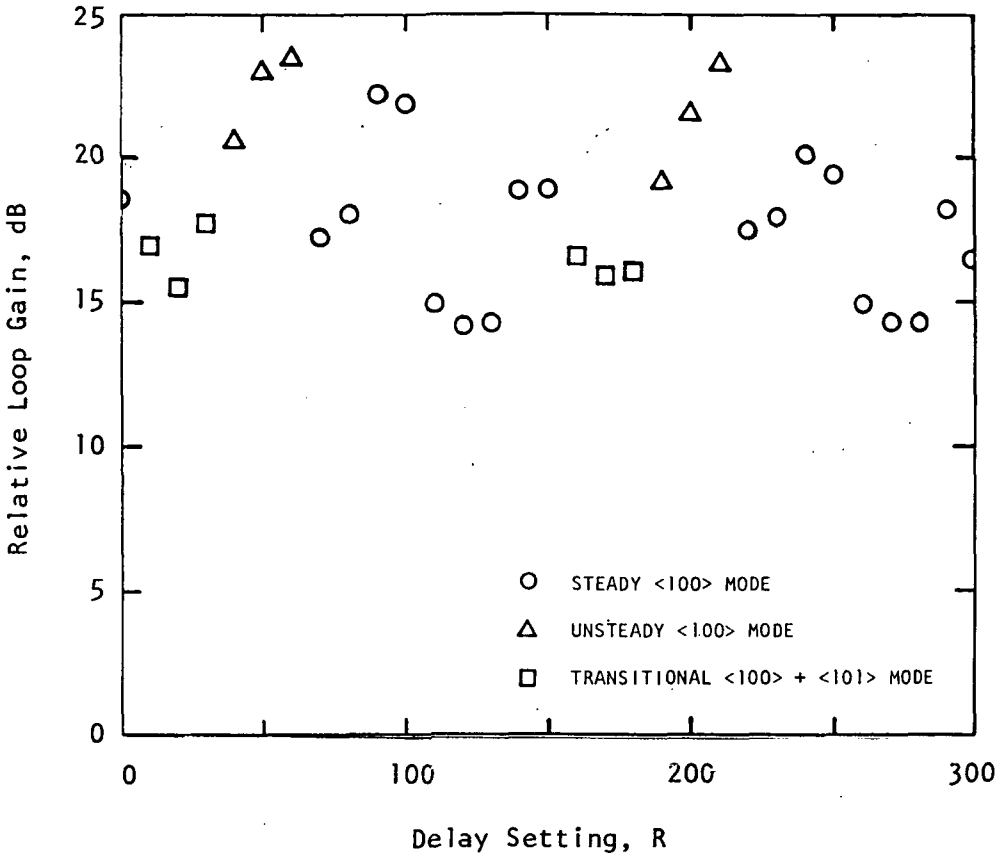

Figure 19. Map of Minimum Relative Loop Gain Necessary for Self-Sustained CTHWA Closed-Loop Operation—T = 25°C; Initial Acoustic Field = <100> with L_p = 153.8 dB

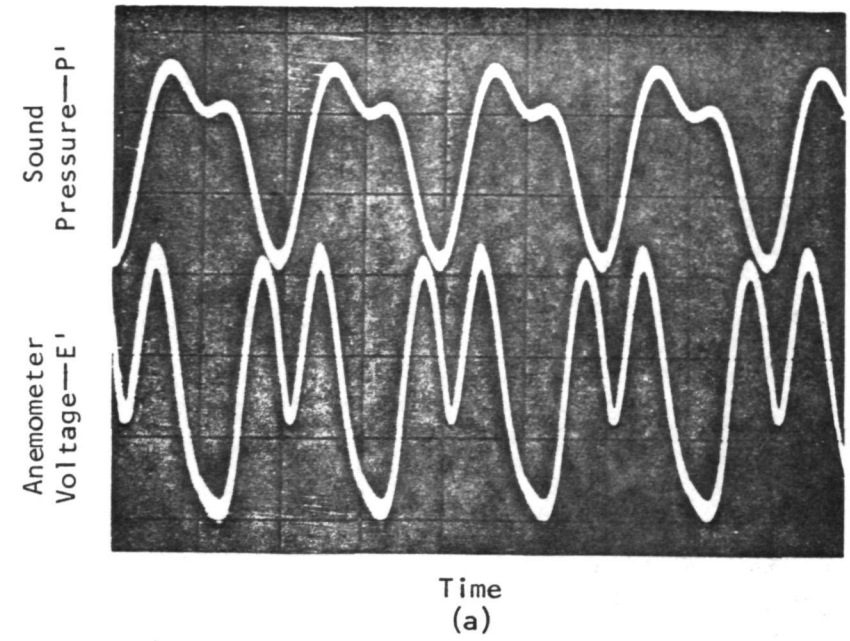

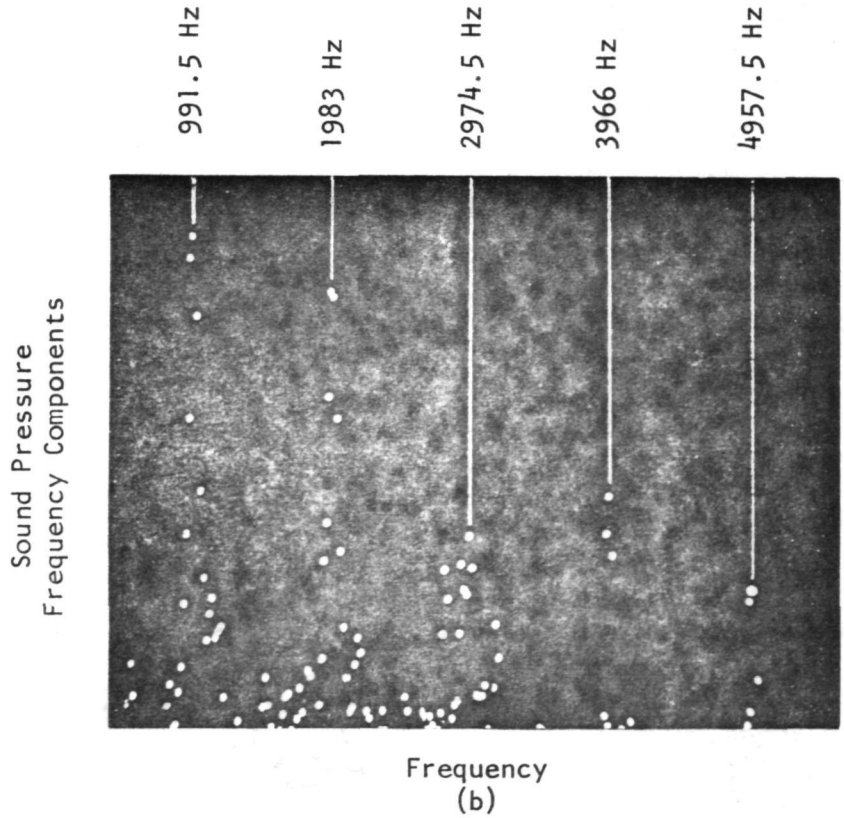

Figure 20. Steady Self-Sustained CTHWA Closed-Loop Phenomenon—T = 26^{0}C; R = 270

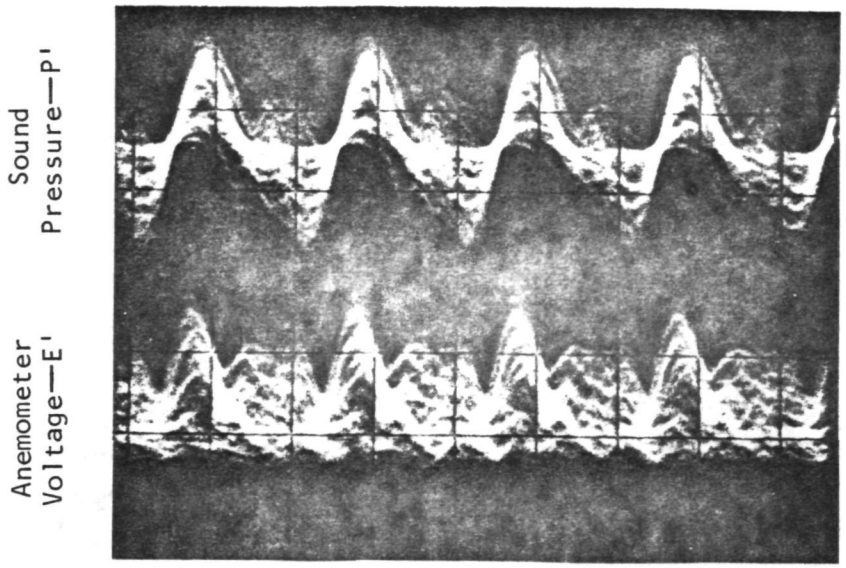

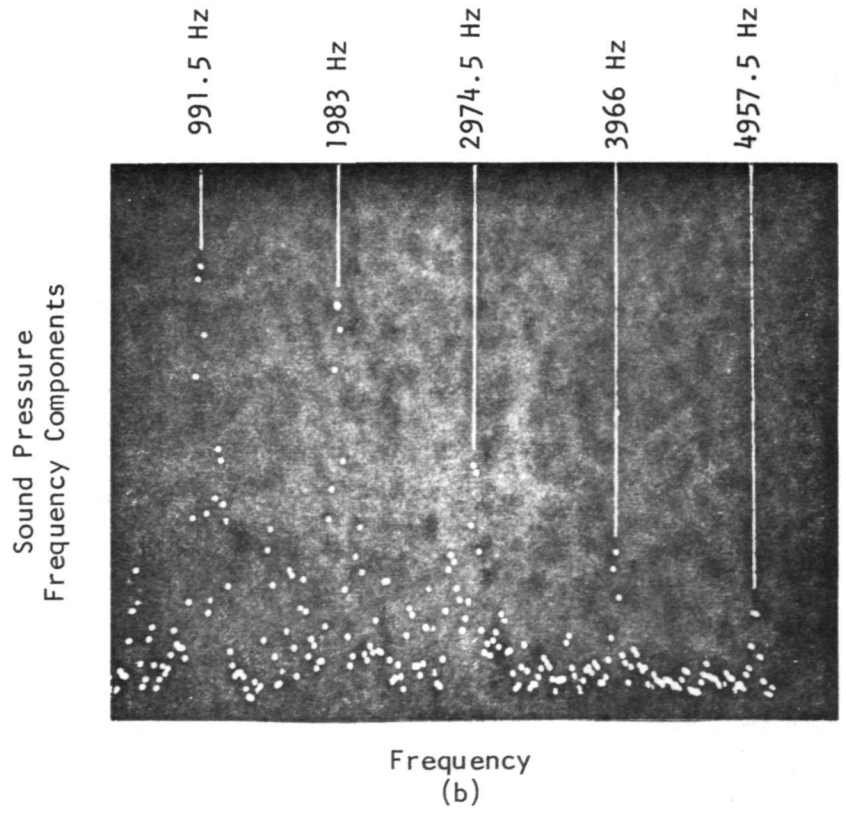

Figure 21. Unsteady Self-Sustained CTHWA Closed-Loop Phenomenon—T = 26^0C; R = 200

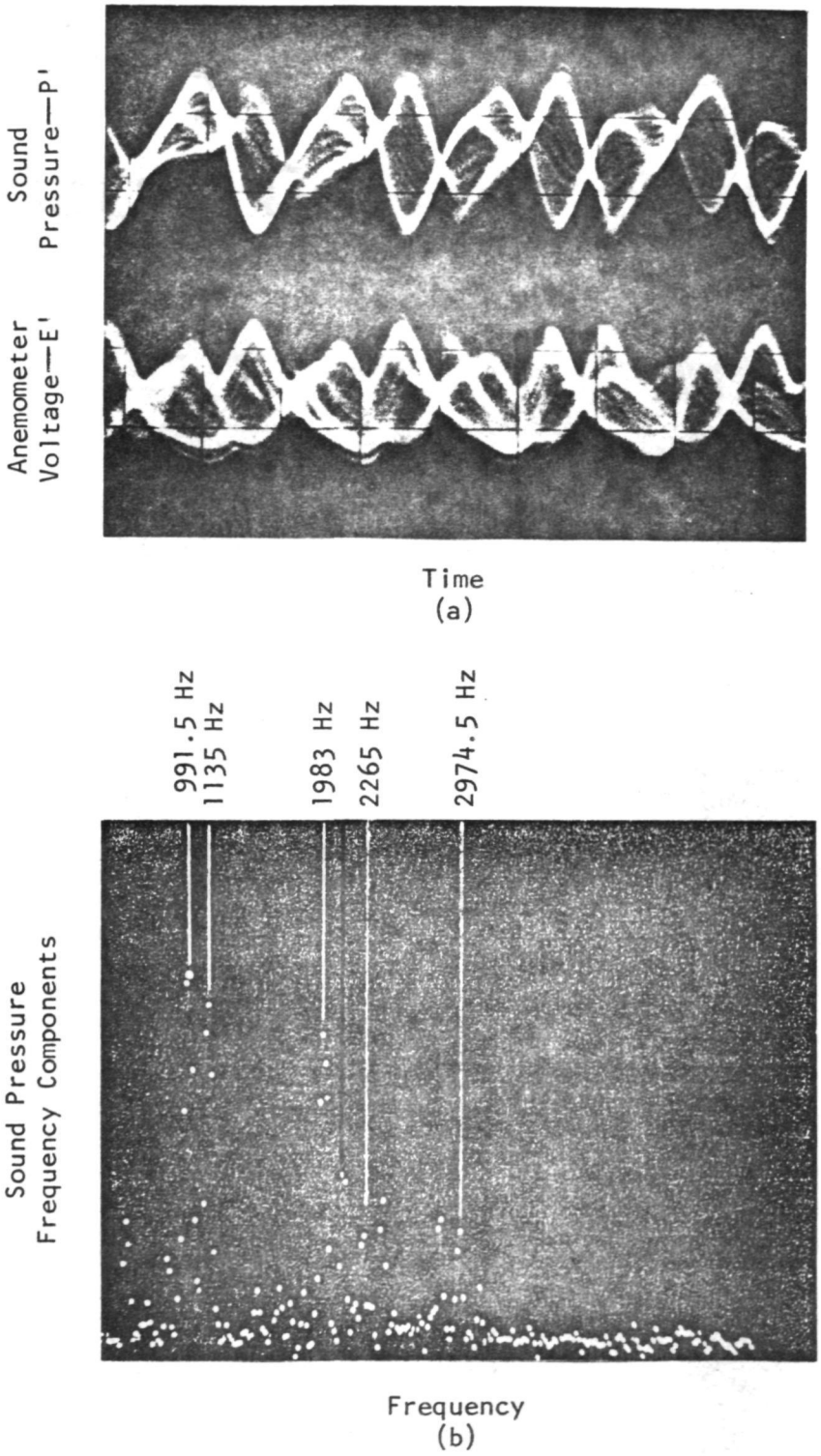

Figure 22. Transitional Self-Sustained CTHWA Closed-Loop Phenomenon—T = 26^{0}C; R = 170

calculations of the total phase shift through the loop ψ_{TOTAL} and the analytical results previously presented concerning the frequency components of the CTHWA in response to certain combined acoustic fields. From the closed-loop electrical path shown in figure 6, the total phase shift through the CTHWA closed-loop can be shown to be

$$\psi_{TOTAL} = \psi_{P/D} + \psi_{E/P} + \psi_{C7} + \psi_{VA} + \psi_{PA} - 360\ n \qquad (26)$$

(Again, the purpose of the last term is to reduce ψ_{TOTAL} to a value between 0 and 360 degrees.)

At R = 120, ψ_{TOTAL} for the <100> and <202> frequency components of the feedback signal was very close to being a complete cycle and, in agreement with this, a relatively small amount of amplification was needed for self-sustenance and the waveform was very steady. Likewise, at R = 270, ψ_{TOTAL} for the <100> and <202> frequency components was very close to being a complete cycle and the amplification needed for self-sustenance was low and the waveform steady.

Changing the time delay setting to R = 140 causes ψ_{TOTAL} for the <100> and <202> frequency components to change to 38 and 77 degrees respectively. The waveform remained steady since the deviation from the optimum setting was still small; however, more amplification was needed than at the optimum locations of R = 120 and 270.

Increasing R to 170 changed ψ_{TOTAL} for the <100> and <202> frequency components to 110 and 219 degrees respectively. Following the previous logic, this should have caused the required gain for self-sustenance to be high; however, at this setting the <101> and <300> frequency components had ψ_{TOTAL}'s close to zero so that the required

gain for self-sustenance decreased. (The frequency of the <300> acoustic field is close to, but is not exactly, twice that of the <101> acoustic field.)

At a time delay setting of R = 210, ψ_{TOTAL} for the <100> and <202> frequency components was 184 and 9 degrees, respectively. The <202> was in phase, but the <100> was out of phase; hence, a large amount of gain was required for self-sustenance. When an existing and a feedback acoustic field are out of phase, the feedback acoustic field must be stronger than the existing field if self-sustenance is to be attained. The acoustic fields will constantly interfere with each other; therefore, the level of the self-sustained field will be unsteady, as is indicated in figure 21.

At a time delay setting of R = 220—a relative minimum region— ψ_{TOTAL} for the <100> frequency component was 231 degrees and that for the <202> frequency component was 103 degrees. These both deviated significantly from 180 degrees; therefore, more gain was required than at the optimum locations, but less gain was required than was needed when ψ_{TOTAL} was 184 degrees for the <100> frequency component.

When the time delay setting was increased to R = 240, ψ_{TOTAL} for the <202> frequency component was close to 180 degrees; hence, the amount of gain needed for self-sustenance increased.

When the time delay setting reached R = 270, one cycle for the <100> frequency component and two cycles for the <202> frequency component had been traversed and the pattern repeated itself.

In the CTHWA closed-loop experiments, the <100> plus <202> acoustic fields always developed. This was a natural result of the nonlinearity of the system and the dimensions of the chamber. When

the system was excited at a resonant frequency, the output from the CTHWA was predominantly composed of a second harmonic component plus higher even harmonics. Since the doubled frequency component was at a resonant frequency, when it was fed back to the chamber, the chamber responded strongly to it. At this stage the acoustic oscillation at the doubled frequency combined with the acoustic oscillation at the fundamental frequency. Such a combination resulted in a CTHWA output having strong components at both the fundamental and the doubled frequencies. (This was brought out by the fourier analysis presented earlier—figures 7, 8 and 9.) From then on both frequencies appeared in the feedback signal. If the doubled frequency had not been a resonant frequency (or close to a resonant frequency, as in the case of f_{101} and f_{300}) the system could not sustain itself. Driving a non-resonant frequency would require too much power for it to be self-sustaining. (The microphone closed-loop studies confirmed that the system responds to resonant frequencies, even if the feedback signal is not exactly in phase with the previous signal.)

In the microphone closed-loop experiments, the <202> acoustic field did not appear, except as a lesser component of the signal which was dominated by a resonant acoustic field which required less power to drive. In the CTHWA experiments the <202> acoustic field played a dominant role due to the fact that $f_{202} = 2f_{100}$.

The above statements concerning the necessity of having two resonant frequencies such that one was twice the other, in order to have self-sustenance, was verified by altering the length of the chamber so that the condition did not exist. With the altered chamber there was no value of time delay for which it was possible to obtain

self-sustained closed-loop operation with even very large amounts of gain in the loop.

In summary, closed-loop self-sustained operation using the CTHWA was found to be dependent upon the existence of two resonant frequencies, one of which was twice (or close to twice) the frequency of the other. The frequencies which developed were dependent upon the amount of time delay in the loop and the resonant frequencies of the chamber. (The resonant frequencies were a function of the length and the diameter of the chamber.) The resultant frequencies were always harmonics of each other. The closer the total time delay through the loop was to being a complete cycle for each frequency component, the lower was the gain required for self-sustenance. When the required resonant frequencies existed, closed-loop operation could be sustained for any amount of time delay, provided there was sufficient amplification; however, the operating characteristics changed considerably with changes in time delay. For some conditions the resulting closed-loop operation was very steady; for other conditions it was very unsteady. Rayleigh's criterion [4] was the dominant factor controlling the response of the system during closed-loop operation.

CONCLUSIONS

A distorted acoustic field is a natural result of a nonlinear feedback system. The nonlinear response to, or feedback from, a sinusoidal disturbance of frequency f is a signal with a strong frequency component at 2f. When the signal at 2f is fed back and added to the disturbance at f, the resultant disturbance has strong frequency components at f and 2f, provided the chamber can respond strongly to a

signal at 2f. To maintain or amplify the acoustic field in a closed-loop situation, such as was studied here, the feedback signal should match as closely as possible the frequencies and phases of the existing acoustic field so that when added, they can reinforce each other. Adding a signal at 2f to a signal at f results in a signal containing strong components at both f and 2f. A nonlinear system naturally generates both the doubled and the fundamental frequencies. If both frequencies are resonant (or close to resonant) frequencies, the system can sustain or amplify the disturbance, provided sufficient gain exists.

Since it is natural to generate second-harmonically distorted acoustic vibrations with a nonlinear system, it is probable that the coupling between the burning process in a liquid-propellant rocket engine and the gas dynamic variables of the system is velocity sensitive rather than pressure sensitive. (Pressure coupling is linear and does not naturally develop a distorted disturbance from a sinusoidal perturbation unless the acoustic field is very "strong.")

To aid in the suppression of acoustic instability in a rocket engine, the length (or diameter) of the chamber should be adjusted so that none of the lower resonant-mode frequencies differ by a factor of two.

Analyzing the situation, a pressure disturbance caused by the unsteady burning of a fuel droplet at one location (a pressure antinodal location) causes the maximum velocity perturbation (velocity antinode) at another location in the chamber. Thus a droplet's environment is in part produced by the unsteady burning of a fuel droplet some distance away. Breaking up the communication between these two locations, such as is done with a baffle, should suppress

the interaction and thereby either prevent an instability from developing or alter its type.

LIST OF REFERENCES

1. Priem, R. J. and M. F. Heidmann, "Propellant Vaporization as a Design Criterion for Rocket-Engine Combustion Chambers," NASA TR R-67, 1960.

2. Collis, D. C. and M. J. Williams, "Two-Dimensional Convection from Heated Wires at Low Reynolds Numbers," J. Fluid Mech., 6, pp. 357-384, 1959.

3. Fang, J. C., On the Convection Limited Self-Sustained Acoustic Vibrations in a Closed-Closed Cylindrical Chamber, Ph.D. Dissertation, College of Engineering, Tennessee Technological University, 1975.

4. Rayleigh, J. W. S., The Theory of Sound, Vol. II, Dover Publications, New York, pp. 226-227, 1945.

5. Heidmann, M. F., "Amplification by Wave Distortion of the Dynamic Response of Vaporization Limited Combustion," NASA TN D-6287, May 1971.

6. Purdy, K. R., M. B. Ventrice and J. C. Fang, "An Investigation of the Open-Loop Amplification of Reynolds Number Dependent Processes by Wave Distortion," Proceedings of the Tenth Southeastern Seminar on Thermal Sciences, pp. 176-204, April 1974.

7. Ventrice, M. B. and K. R. Purdy, "An Investigation of the Open-Loop Amplification of a Reynolds Number Dependent Process by Wave Distortion," NASA CR-134620, May 1974.

8. Fang, J. C. and K. R. Purdy, "Calibration of a Constant-Temperature Hot-Wire Anemometer for Very Low Reynolds Numbers," Mechanical Engineering Report, ME-44, Tennessee Technological University, Dec. 1973.

FINAL REPORT DISTRIBUTION LIST

NASA-Lewis Research Center
Attn: Dr. R. J. Priem/MS 500-204
21000 Brookpark Road
Cleveland, OH 44135
(4 copies)

NASA-Lewis Research Center
Attn: Library/MS 60-3
21000 Brookpark Road
Cleveland, OH 44135

NASA-Lewis Research Center
Attn: Report Control Office/MS 5-5
21000 Brookpark Road
Cleveland, OH 44135

NASA-Lewis Research Center
Attn: E. A. Bourke/MS 500-205
21000 Brookpark Road
Cleveland, OH 44135

NASA Headquarters
Attn: RPS/Robert A. Wasel
600 Independence Ave., SW, Rm 526
Washington, DC 20546

NASA-Lewis Research Center
Attn: 1442/Procurement Officer
Mail Stop 500-313
21000 Brookpark Road
Cleveland, OH 44135

NASA-Lyndon B. Johnson Space Center
Attn: EP/Joseph G. Thibodaux
Houston, TX 77058

NASA-George C. Marshall Space Flight Center
Attn: S&E-ASTN-PP/R. J. Richmond
Huntsville, AL 35812

NASA Scientific & Technical Info. Facility
Attn: Accessioning Department
P. O. Box 8757
Balt/Wash International Airport
Maryland 21240 (10 copies)

Aerojet Liquid Rocket Company
Attn: David A. Fairchild
Bldg. 20001/Sec. 9732
P. O. Box 13222
Sacramento, CA 95813

Aerospace Corporation
Attn: O. W. Dykema
P. O. Box 92957
Los Angeles, CA 90045

Air Force Rocket Propulsion Lab (RPM)
Attn: Library
Edwards, CA 93523

Air Force Office of Scientific Research
Chief Propulsion Division
Attn: Dr. J. F. Masi (NAE)
1400 Wilson Boulevard
Arlington, VA 22209

Air Force Rocket Propulsion Laboratory
Attn: Daweel George
Edwards, CA 93523

Air Force Rocket Propulsion Laboratory
Attn: Richard R. Weiss
Edwards, CA 93523

AFAPL
Attn: Frank D. Stull (RJT)
Wright Patterson AFB, OH 45433

Army Ballistics Research Labs
Attn: Austin W. Barrows
Code AMXBR-1B
Aberdeen Proving Grounds, MD 21005

Army Ballistic Research Labs
Attn: Ingo W. May
Code AMXBR-1B
Aberdeen Proving Grounds, MD 21005

Army Material Command
Missile Systems Division
Attn: Stephen R. Matos
Code AMCRD-MT
5001 Eisenhower Avenue
Alexandria, VA 22304

Bell Aerospace Company
Attn: T. F. Ferger
Post Office Box 1
Mail Zone, J-81
Buffalo, NY 14205

Brooklyn Polytechnic Institute
Long Island Graduate Center
Attn: V. D. Agosta
Route 110
Farmingdale, NY 11735

California Institute of Technology
Jet Propulsion Laboratory
Attn: Fred E. C. Culick
4800 Oak Grove Drive
Pasadena, CA 91103

California Institute of Technology
Jet Propulsion Laboratory
Attn: Jack H. Rupe
4800 Oak Grove Drive
Pasadena, CA 91103

California State University Sacramento
School of Engineering
Attn: Frederick H. Reardon
6000 J. Street
Sacramento, CA 95819

Chemical Propulsion Information Agency
Johns Hopkins University/APL
Attn: T. W. Christian
Johns Hopkins Road
Laurel, MD 20810

Colorado State University
Attn: Charles E. Mitchell
Fort Collins, CO 80521

Frankford Arsenal
Attn: Martin Visnov
NDP-R, Bldg. 64-2
Bridge & Tacony Streets
Philadelphia, PA 19137

General Electric Company
Flight Propulsion Laboratory Dept.
Attn: D. Suichu
Cincinnati, OH 45215

Georgia Institute of Technology
Georgia Tech. Res. Institute
Attn: Warren C. Strahle
Atlanta, GA 30332

Georgia Institute of Technology
Georgia Tech. Res. Institute
Attn: Ben T. Zinn
Atlanta, GA 30322

Melvin Gerstein
P. O. Box 452
Altadena, CA 91001

Massachusetts Institute of Technology
Department of Mechanical Engineering
Attn: T. Y. Toong
77 Massachusetts Avenue
Cambridge, MA 02139

McDonald Douglas Corporation
McDonnell Douglas Astronautics Co.
Attn: William T. Webber
5301 Bolsa Avenue
Huntington Beach, CA 92647

Lockheed Aircraft Corporation
Lockheed Propulsion Co., Div.
Attn: Norman S. Cohen
P. O. Box 111
Redlands, CA 92373

Naval Postgraduate School
Department of Aeronautics
Attn: David W. Netzer
Monterey, CA 93940

Naval Underwater Systems Center
Energy Conversion Dept.
Attn: Robert S. Lazar, Code 5B331
Newport, RI 02840

Naval Weapons Center
Attn: Edward W. Price, Code 608
China Lake, CA 93555

Naval Weapons Center
Attn: Charles J. Thelen, Code 4505
China Lake, CA 93555

Pennsylvania State University
Mechanical Engineering Department
Attn: G. M. Faeth
207 Mechanical Engineering Bldg.
University Park, PA 16802

Princeton University
Forrestal Campus Library
Attn: Irvin Glassman
P. O. Box 710
Princeton, NJ 08450

Princeton University
Forrestal Campus Library
Attn: David T. Harrje
P. O. Box 710
Princeton, NJ 08540

Princeton University
Forrestal Campus Library
Attn: Martin Summerfield
P. O. Box 710
Princeton, NJ 08540

Purdue University
Jet Propulsion Laboratory
Project Squid
Attn: Robert Goulard
West Lafayette, IN 47907

Purdue University Research Foundation
School of Mechanical Engineering
Attn: John R. Osborn
Thermal Science Propulsion Center
West Lafayette, IN 47906

Purdue University Research Foundation
School of Mechanical Engineering
Attn: Bruce A. Reese
Thermal Science Propulsion Center
West Lafayette, IN 47906

Research and Development Associates
Attn: Raymond B. Edelman
P. O. Box 3580
525 Wilshire Blvd.
Santa Monica, CA 90402

Rockwell International Corporation
Rocketdyne Division
Attn: L. P. Combs, D/991-350
Zone 11
6633 Canoga Avenue
Canoga Park, CA 91304

Rockwell International Corporation
Rocketdyne Division
Attn: James A. Nestlerode
Dept. 596-124, AC46
6633 Canoga Avenue
Canoga Park, CA 91304

Rockwell International Corporation
Rocketdyne Division
Attn: Carl L. Oberg
Dept. 589-197-SS11
6633 Canoga Avenue
Canoga Park, CA 91304

TISIA
Defense Documentation Center
Cameron Station, Bldg. 5
5010 Duke Street
Alexandria, VA 22314

Tennessee Technological University
College of Engineering
Attn: Kenneth R. Purdy
P. O. Box 5005
Cookeville, TN 38501

TRW Systems
Attn: G. W. Elverun
One Space Park
Redondo Beach, CA 90278

Tulane University
Attn: J. C. O'Hara
6823 St. Charles Avenue
New Orleans, LA 70118

Ultrasystems, Inc.
Attn: Thomas J. Tyson
500 Newport Center Drive
Newport Beach, CA

United Aircraft Corporation
Pratt & Whitney Aircraft Division
Attn: Thomas C. Mayes
P. O. Box 2691
West Palm Beach, FL 33402

United Aircraft Corporation
Attn: R. H. Woodward Waesche
400 Main Street
East Hartford, CT 06108

University of California
Aerospace Engineering Dept.
Attn: F. A. Williams
Post Office Box 109
LaJolla, CA 92037

University of California, Berkeley
Department of Mechanical Engineering
Attn: A. K. Oppenheim
Berkeley, CA 94720

University of Illinois
Aeronautics/Astronautic Engr. Dept.
Attn: R. A. Strehlow
Transportation Bldg., Room 101
Urbana, IL 61801

University of Michigan
Attn: James A. Nicholls
P. O. Box 622
Ann Arbor, MI 48107

University of Utah
Department of Chemical Engineering
Attn: Alva D. Baer
Park Bldg., Room 307
Salt Lake City, UT 84112

University of Wisconsin
Mechanical Engineering Department
Attn: P. S. Myers
1513 University Avenue
Madison, WI 53706

Virginia Polytechnic Institute
State University
Attn: J. A. Schetz
Blacksburg, VA 24061